
# Full-Wave Based Validation of Stripline Field Applicator for Low Frequency Material Measurements

THESIS

James H. Crane, II, Captain, USAF

AFIT/GE/ENG/09-10

**DEPARTMENT OF THE AIR FORCE**
**AIR UNIVERSITY**

***AIR FORCE INSTITUTE OF TECHNOLOGY***

**Wright-Patterson Air Force Base, Ohio**

The views expressed in this thesis are those of the author and do not reflect the official policy or position of the United States Air Force, Department of Defense, or the United States Government.

AFIT/GE/ENG/09-10

# Full-Wave Based Validation of Stripline Field Applicator for Low Frequency Material Measurements

THESIS

Presented to the Faculty

Department of Electrical and Computer Engineering

Graduate School of Engineering and Management

Air Force Institute of Technology

Air University

Air Education and Training Command

In Partial Fulfillment of the Requirements for the

Degree of Master of Science in Electrical Engineering

James H. Crane, II, B.S.E.E.

Captain, USAF

March 2009

AFIT/GE/ENG/09-10

# Full-Wave Based Validation of Stripline Field Applicator for Low Frequency Material Measurements

James H. Crane, II, B.S.E.E.
Captain, USAF

Approved:

| | |
|---|---|
| /signed/ | 19 Mar 2009 |
| Dr. Havrilla, PhD (Chairman) | date |
| /signed/ | 19 Mar 2009 |
| Dr. Collins (Member) | date |
| /signed/ | 19 Mar 2009 |
| Dr. Baker (Member) | date |

# *Abstract*

This research presents the analysis and verification of a stripline designed by Air Force Research Laboratory for use in measuring the electrical properties of materials at low frequencies and high temperature. It is designed to operate in the TEM mode up to 4 Ghz and have a characteristic impedance of 50 ohms. A full wave base method is used to analyze the structure. The parallel plate waveguide dyadic Green's function is developed for a current immersed in a PEC parallel plate environment. It is used to formulate a pair of coupled electric field integral equations (CIE). These CIEs are solved through a computationally efficient entire-domain method of moments (MoM) technique. Numerical efficiency is gained through employing Chebsyshev polynomials of the first and second kind as testing and expansion functions. These efficient expansion and testing function sets require as few as three expansions for accurate results. Further numerical efficiencies are gained by taking advantage of transverse electromagnetic propagation properties to develop a specialized TEM integral equation reducing the number of integrations performed from $2N^2+N$ to $N^2$. An expression for the characteristic impedance is developed using the MoM results. The characteristic impedance is calculated for various degrees of center conductor miss alignment.

*Acknowledgements*

It would not have been possible for me to complete this thesis without the support of many people. I would first like to thank the members of my thesis committee for their time and insight. In addition to those who guided me academically, the support of my friends and family has been equally important. Special thanks go to my wife for always pretending to be interested in the research I was conducting.

James H. Crane, II

*Table of Contents*

Page

# *List of Figures*

# *List of Tables*

## *List of Abbreviations*

# Full-Wave Based Validation of Stripline Field Applicator for Low Frequency Material Measurements

# I. Introduction

## *1.1 Problem Statement*

The objectives of this research are to validate the design parameters of a high temperature/low frequency stripline apparatus developed for the Air Force Research Laboratory using a full-wave analysis and to predict the effects of center conductor misalignment on the characteristic impedance of the apparatus used in material characterization measurements.

## *1.2 Motivation for Stripline Use*

Current material testing at low frequencies requires waveguides having large cross-sectional dimensions (e.g. four feet wide by two feet high). Fabricating samples this large is costly and exceedingly difficult. In addition, obtaining an oven to heat this waveguide/sample fixture would require enormous space and power, making it virtually impossible to implement. The proposed stripline design would have cross-sectional dimensions of approximately five inches by two inches, thus samples are easily fabricated and pre-existing furnaces can easily be used. Thus, the stripline fixture will, for the first time, give Air Force Research Laboratory the capability of measuring shielding material at low frequencies and high temperatures. AFRL's approximate design specifications stipulate that a 50 ohm stripline can be realized if ground plane spacing is approximately 3.5 cm and center conductor width is approximately 5 cm. A full-wave analysis will be developed in this research to more precisely validate the design.

### *1.3 Motivation for Investigating Center Conductor Misalignment*

Striplines used to characterize the properties of materials are air-filled to allow sample insertion. The unsupported center-conductor often sags (see figure 1.1) leading to characteristic impedance, $Z_0$, uncertainty. It has been found that permittivity and permeability measurements are highly susceptible to S-parameter and $Z_0$ uncertainty [2, 18]. Better characterization can be achieved with an expression for $Z_0$ that can accommodate center-conductor misalignment. Previous techniques include conformal mapping, finite difference equations and various Green's function/integral equation methods. While conformal mapping yields exact results, it involves complicated functions and is cumbersome to implement especially when the system is not symmetric. The finite difference technique requires evaluation points on the order of 5,000-10,000, making it computationally intensive [25]. Integral equation approaches, like Kammler's, lower computational size by using a sub-domain method of moments technique. Approximate methods are also presented in the literature [20, 31]. The goals of this research is to develop a full-wave, computationally efficient expression for computing $Z_0$ of a stripline having a misaligned center conductor.

### *1.4 Limitations*

In order to make the problem tractable a simplified model of the stripline has been assumed. The geometry is considered to be invariant along the guiding axis and the center conductor is modeled as an infinitesimally thin strip. In addition, only pre-existing numerical algorithms in Matlab are used for numerical integration. The numerical integration techniques implemented in this research are an adaptive Simpson quadrature, the trapezoidal method, an adaptive Lobatto quadrature, and adaptive Gauss-Kronrod quadrature. These various methods are used to accommodate the various forms of integrals encountered in this research.

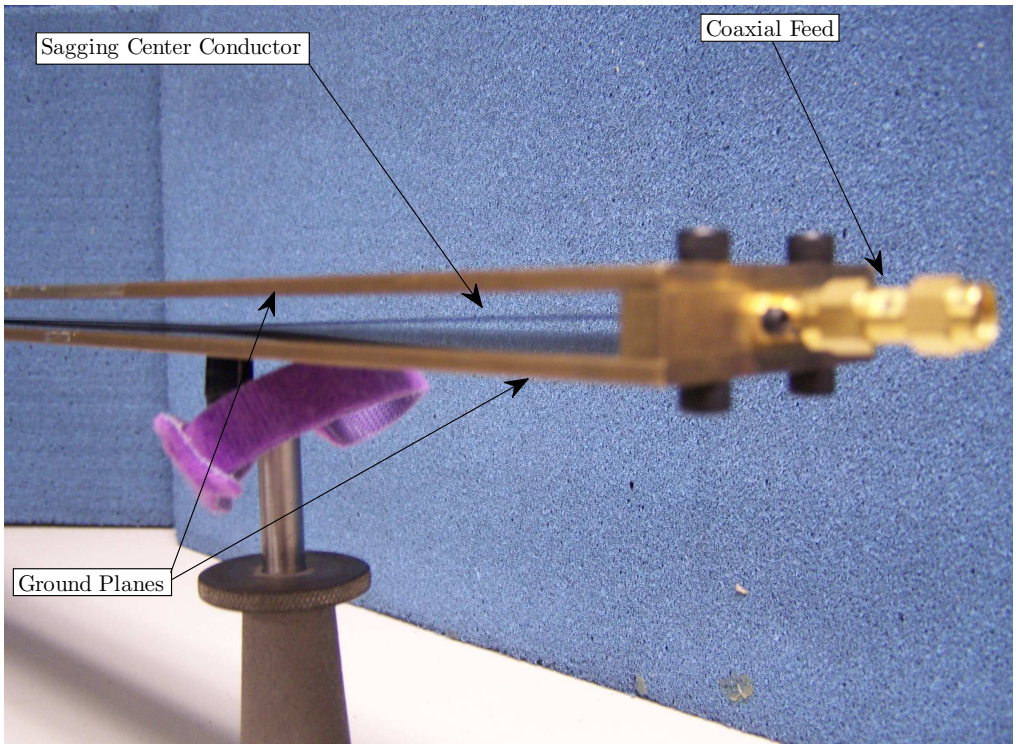


Figure 1.1: Example of center conductor sag.

## *1.5 Scope*

There are certainly other methods to validate the physical parameters of a stripline and investigate its characteristic impedance, as mentioned previously. This thesis focuses on an integral equation formulation based on a parallel plate Green's function and efficient entire domain method of moments solution for the center strip current. The ground planes are modeled as perfect electric conductors (PECs). Also, as stated in Section 1.4, the center conductor is modeled as infinitesimally thin and the structure is considered invariant along the guiding axis.

## *1.6 Organization*

Chapter 2 provides the necessary theoretic background starting with an overview of transmission line theory, stripline design and applications. Chapter 3 provides the development of the required parallel plate vector potential Green's function. Chapter 4 details the formulation of a generalized pair of coupled electric field integral equations (EFIE's). It includes the development of a specialization for the transverse electromagnetic (TEM) propagating mode. Chapter 5 details the Method of Moments (MoM) solution for the general and specialized integral equation cases. It will include a discussion on the type of expansion and testing functions selected and conclude with numerical results. In Chapter 6, the characteristic impedance of the stripline will be investigated for various center strip alignment configurations. Proposed design parameters will be validated using this information. Lastly, the thesis concludes in Chapter 7 with a summary of research efforts, results, potential contributions and future research opportunities.

# II. Background

The purpose of this chapter is to provide a background for the stripline field applicator, and to explore current research efforts in this topic. It is assumed that the reader is familiar with electromagnetic theory and the uses and application of Maxwell's equations. This chapter will look at basic transmission line theory, basic stripline characteristics and design practices, applications in material characterization and current efforts to mitigate characterization error resulting from characteristic impedance uncertainty.

## *2.1 Transmission Line Theory*

The stripline belongs to a family of devices called transmission lines. A transmission line is a structure that forms all or part of a path from one place to another for directing the transmission of energy, such as electromagnetic waves or acoustic waves, as well as electric power transmission [31]. Moreover, in electromagnetics, a transmission line is comprised of conductors linking electrical systems that guide energy. Additional examples of transmission lines include wires, coaxial cables, electric power lines, and microstrips. Transmission line theory must be used when the length of the devices to be analyzed is long with respect to the operational wavelength. This relatively large size allows for variation in voltage and current distributed throughout the system or circuit.

A distributed model for a section of transmissions line is shown in the Figure 2.1 where $R$ is the resistance in both conductors per unit length ($\Omega/m$), $L$ is the inductance in both conductors per unit length ($H/m$), $G$ is the conductance of the dielectric media per unit length ($S/m$) and $C$ is the capacitance between the conductors per unit length ($F/m$). [24] $R$ is included to account for ohmic losses in the line. $G$ is included to account for dielectric losses in the dielectric between conductors. $L$ and $C$ are included to account for the electric and magnetic energy stored in the line [23]. For lossless lines R and G are zero. This model can be used to find fundamental transmission line properties, namely the propagation constant and the

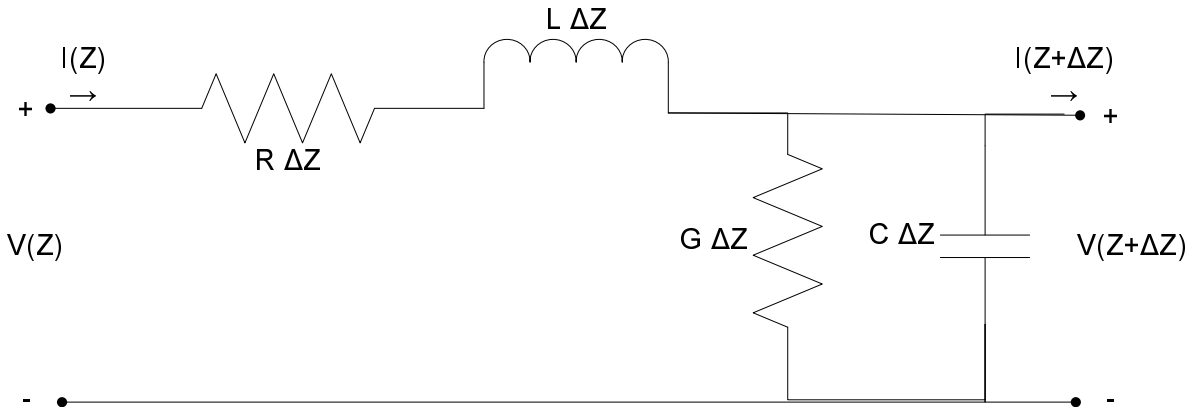


Figure 2.1: Model for transmission line using circuit components.

characteristic impedance. The propagation constant , $\gamma = \alpha + j\beta$, is calculated in terms of the inductance, capacitance, conductance and resistance of the line and is given by the expression [23]

$$\gamma = j\omega\sqrt{(R + j\omega L)(G + j\omega C)} \tag{2.1}$$

If the line is lossless ($R, G = 0$), the propagating constant is purely imaginary. For TEM modes, the wave number, $k$, is related to the propagating constant according to the following relation

$$\gamma = jk \tag{2.2}$$

where

$$k = \beta - j\alpha \tag{2.3}$$

and behaves like

$$e^{-\gamma z} = e^{-jkz} = e^{-\alpha z}e^{-j\beta z} \tag{2.4}$$

with $\alpha = 0$ for a lossless line. The characteristic impedance of a transmission lines is the ratio of the voltage to the current for a single traveling wave. The characteristic impedance has units of ohms and is given as

$$Z_o = \pm \frac{V_o^{\pm}}{I_o^{\pm}} = \sqrt{\frac{R + j\omega L}{G + j\omega C}} \tag{2.5}$$

When using transmission lines in conjunction with other devices (i.e. Generators, loads or other transmission lines) the behavior of the energy at the junctions is important to understand. For maximum power transfer, the impedance of all devices in a system must be matched. Variations in the impedance results in reflections. The ratio of forward traveling energy to reflected energy is known as the reflection coefficient. The reflection coefficient, expressed in terms of characteristic impedance, is given by

$$\Gamma = \frac{Z_L - Z_0}{Z_L + Z_0}, \tag{2.6}$$

where $Z_L$ is the load impedance and $Z_0$ is the characteristic impedance of the line.

## *2.2 Stripline*

Since their conception in the 1950's [31] striplines have been carefully studied. Like the coax, the stripline supports a dominant transverse electromagnetic mode. Its geometry is characterized by a metal strip sandwiched between two parallel ground planes. The dominant mode of the stripline is non-dispersive and has zero cutoff frequency. Striplines are also relatively easy to fabricate.

Throughout this research, the following coordinate system will be adopted to describe the stripline geometry. A cross section is illustrated in the Figure 2.2. The origin is placed at the center between the ground planes. The perfect electric conductor (PEC) ground planes located at $y = \pm h$ extend infinitely in the $x$ and $z$

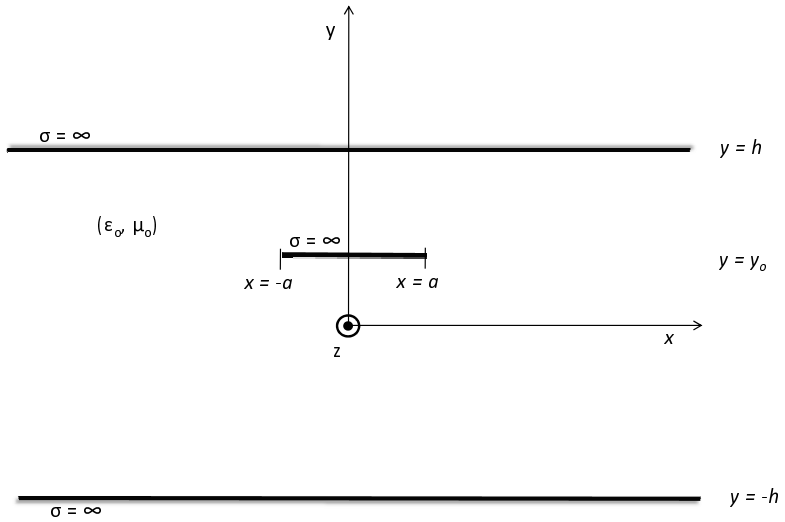


Figure 2.2: Stripline cross section with misaligned center conductor.

directions. The infinitesimally thin center conductor is located at $y = y_o$ and extends from $-a < x < a$.

*2.2.1 Asymmetric Striplines.* A second class of stripline has begun to emerge. This class, referred to as asymmetric striplines, incorporates all stripline that have a non-uniform center conductor or a center conductor that is not perfectly centered between the ground planes. Asymmetry effects the stripline properties presented in previous sections. The effects of the misalignment on characteristic impedance will be explored in Chapter 6.

## *2.3 Stripline Design*

The main considerations for stripline design are selecting materials used in fabrication, calculating physical parameters and devising a method to feed the apparatus. Other key factors are operating frequency regime and characteristic impedance. In

Table 2.1: Property summary of material for center conductor and ground plane fabrication.

| Metal | Conductivity |
|---|---|
| Silver | $6.3 \times 10^7$ |
| Copper | $5.9 \times 10^7$ |
| Gold | $4.5 \times 10^7$ |
| Aluminum | $3.7 \times 10^7$ |
| Tin | $9.17 \times 10^6$ |
| H-214*( at 2200 deg F) | $8.1 \times 10^5$ |
| H-230*(at 1800 deg F) | $7.9 \times 10^7$ |
| HR-120*(at 2200 deg F) | $7.7 \times 10^5$ |
| H-282*(at 1800 deg F) | $7.6 \times 10^7$ |
| * High temperature alloys produced by Haynes International, Inc. | |

this section some of the possible fabrication materials will be reviewed and the method of calculating the physical characteristics of the stripline will be described.

Material selection must begin early in the design process [20]. Careful selection of the dielectric material between the ground planes and the center strip will strongly effect the performance of the stripline. Material uniformity, homogeneity, isotropy, useful temperature range, durability and frequency response are the main factors governing material selection. Table 2.1 lists possible choices for the conductors.

Physical parameters (such as operational frequency and $Z_0$) are governed by the intended use and are typically user defined. The first step in specifying the operational frequency regime of a stripline is to calculate the spacing of the ground planes. The fact that the ground planes form a parallel plate waveguide will be exploited. To ensure that no higher order modes are excited, the cut-off frequency for the first higher order mode above the dominant mode must be set (as a rule of thumb) ten percent above the desired highest frequency of operation. Next, the width of the center conductor must be computed to achieve the desired characteristic impedance. The secondary dimensions of the ground planes, length and width must be selected according to the intended application.

For a stripline that will operate in the dominant mode up to 4 GHz, stripline spacing can be calculated using the following well known expression [11]

$$2h = \frac{c}{2f_{co_1}} \tag{2.7}$$

where $2h$ is the spacing between the ground planes, $c$ is the speed of light in a vacuum and $f_{co_1}$ is the cutoff frequency of the first mode above TEM.

An approximate value for the center conductor width can be found by using the predetermined center conductor width ($a$) to the ground plane spacing ($h$) ratio given by the expression [10]

$$\frac{a}{h} = 1.4 \tag{2.8}$$

More exact results for the width of the center conductor will be computed using a full wave analysis in Chapter 6.

The stripline applicator will be connected to a network analyzer by coax cable during operation. Selection of a feed method and connector type can effect the balance in the system. Mismatches between the characteristic impedance of the stripline and coax cable will introduce error into material characterization measurements. In the Section 2.5 efforts to improve junction design will be explored.

## *2.4 Applications*

Striplines have many applications. They have becomes staples in the test community. Striplines are used to measure the electromagnetic properties of materials and to test the radiated immunity of automobile components. This section briefly summarizes these applications. The next section will discuss efforts to improve the stripline junction design.

*2.4.1 Material Measurements.* Striplines are frequently employed to determine the electromagnetic properties of materials. [9,39] The advent of modern network analyzers has made automated calculation of the constituent parameters possible.

Accurate extraction of the permittivity and permeability of a material require a well calibrated system and reliable extraction methods.

*2.4.1.1 Calibration.* One method of calibrating a 2-port networks is composed of through, reflect and line (TRL) measurements [9]. The thru measurement is accomplished by connecting the ends of the port-1 and port-2 terminals. The reflect measurement is accomplished by connecting a short, or reflecting standard, to each port. For the line measurement, a length of transmission line is inserted between the test ports. This method is very useful in waveguide measurements.

Other test beds pose a challenge to calibration. The TRL method above doesn't lend itself well to the stripline. For stripline calibration, an empty line measurement and three carefully placed shorts provide the information necessary for calibration [9, 39].

*2.4.1.2 Extracting Constitutive Parameters.* The Nicolson-Ross-Wier algorithm (NRW) is used to calculate the permittivity and permeability of unknown materials from forward scattering parameters, S11 and S21, or reverse scattering parameters, S22 and S12 [9]. It is limited to single layered, homogeneous, isotropic materials. For layered material, it is necessary to convert the scattering parameters to wave transmission parameters (A-parameters) and isolate the A-parameters of the unknown layer. Once isolated, the A-parameters of the unknown layer can be converted to S-parameters of the unknown and NRW can be used to find the constituent parameters for the unknown layer [9, 39].

*2.4.2 Automotive Industries Use of the Tri-Plate.* The automobile industry uses a stripline-like device, a tri-plate, to test the radiated immunity of automobile components. The tri-plate generates an electric field between the center plate and the outer plates. As automotive components are place in the tri-plate, the test exposes both the component under test and its wiring harness to the electric field. The operation of the device is monitored as it is exposed to these fields [15].

### *2.5 Efforts to Optimize Striplines*

Mitigating the effects of junction areas has been a major thrust in research, as indicated by the many reference avaliable [6, 15, 16, 27, 30, 32, 34]. A common form of coaxial-to-stripline transition consists of a simple inline butt joint [26, 32]. This junction is not perfectly matched due to the disparity in the dimensions of the two pieces of transmission line. Two approaches to improve impedance matching have been identified in literature, a tapered center conductor and a taper in conjunction with tuning wedges. Similar efforts have been undertaken by the Automobile industries to perfect the tri-plate line [15, 27, 30].

In recounting the design of his measurement device, Barry goes into great detail about his efforts to design the "best possible transition" [6]. The optimal junctions he proposed included a twenty degree taper. These tapers were introduced to avoid capacitances between the conducting strip and conducting plane where the connectors are affixed [34]. Barry's efforts to improve the junction reduced reflections by more than 30 dB [6].

Later, Barry's method was also combined with tuning wedges to further improve impedance matching by Hanson [16]. In this instance an eighteen degree taper was used. Tuning wedges were made by inserting tapered corners at the ends of the ground plane above and below the center conductor. However, Hanson concluded that impedance matching was not critical if the correct method was used to calibrate the system and extract the constitutive parameters. Non-linear tapers and wedges composed of arbitrary permittivity profile have also been used with good results [37].

Tri-plates incorporate a tapered center ground plane and a wedge shaped transition area. Hwang carefully analyzed the impact that the length of the transition zone and the steepness of the wedge have on energy transmission [21]. He determined that at low frequencies, reflections are dominated by the difference in height between the feed and test region of the apparatus. He proposed that a gradual discrete taper would provide the best matching.

## *2.6 Summary*

In this chapter, fundament concepts from transmission theory were summarized. The properties of striplines were examined. Additionally, the stripline design process and a few stripline applications were presented. The chapter concluded with a brief summary of recent developments in stripline fabrication. The information in this chapter will be used throughout the rest of this thesis. The geometry described in Figure 2.2 will be used in the next chapter to develop the parallel plate Green's function. The approximate values for the ground plane spacing and the center conductor width will be refined in Chapter 6.

# III. Parallel−Plate Green's Function Development

## *3.1 Introduction*

This chapter summarizes the derivation of the vector potential Green's function for an electric current immersed in a PEC parallel-plate waveguide, as seen in Figure 3.1. The derivation draws heavily upon the work in [17, 22].

The vector potential parallel plate Green's function is derived by first finding the boundary conditions in terms of vector potential. Next, the general solution of the vector potential wave equation is found. Finally, boundary conditions are enforced on the general solution leading to a unique representation of the vector potential in terms of the Green's function and the electric current. Each of these steps is summarized below.

## *3.2 Vector Potential Boundary Conditions*

Enforcing boundary conditions (BCs) on the electric field (3.1) is complicated by the required gradient and divergence operators [5],

$$\vec{E} = \frac{1}{j\omega\mu\epsilon}(k^2 + \nabla\nabla\cdot)\vec{A}. \tag{3.1}$$

However, these operations can be avoided by recasting the BCs in terms of the vector potential. This is done by taking advantage of the non-coupling nature of a current in a planar PEC environment ( i.e., each component of current maintains only its respective component of potential) [17]. The vector potential BCs are found to be

$$A_x(x, y = \pm h, z) = 0 \quad \forall \quad x, z \tag{3.2}$$

$$\frac{\partial A_y(x, y = \pm h, z)}{\partial y} = 0 \quad \forall \quad x, z \tag{3.3}$$

$$A_z(x, y = \pm h, z) = 0 \quad \forall \quad x, z \tag{3.4}$$

Since the BC's presented in equations (3.2)-(3.4) must hold for all values of $x$, $z$ (i.e., $-\infty < x < \infty$, $-\infty < z < \infty$), a Fourier transformation on these spatial

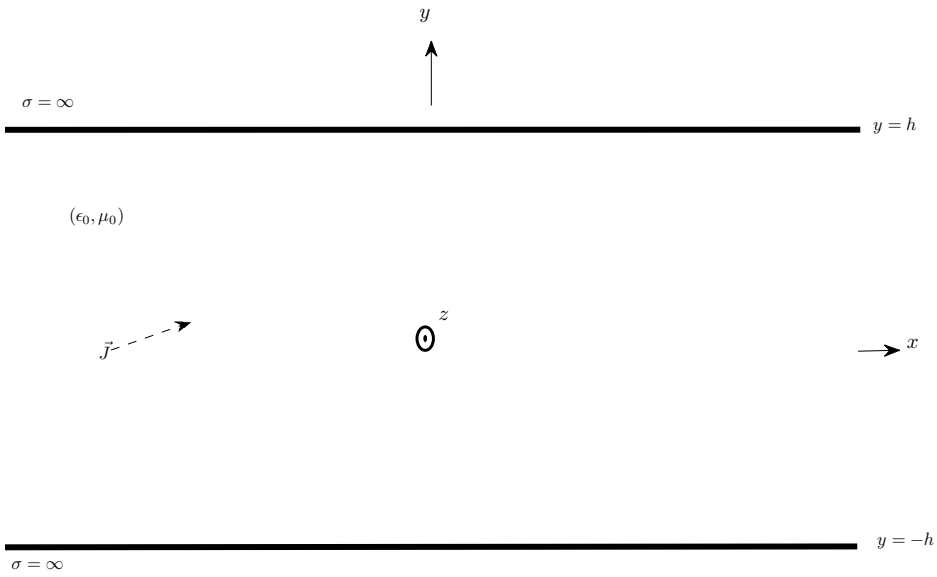


Figure 3.1: Problem Geometry: General 3D Current ($\vec{J}$) Immersed in Parallel Plate Waveguide.

variables is performed. Transforms will be performed according to the defined forms below (see equations (3.5) and (3.6) ). Spectral functions are indicated by a tilde overbar and functional dependance on spectral variables ($x \to \xi, y \to \eta$ and $z \to \zeta$). A double transform is equivalent to two single transforms.

$$\tilde{f}(x,y,\zeta) = \int_{-\infty}^{\infty} f(x,y,z)e^{-jz\zeta}dz \Leftrightarrow f(x,y,z) = \frac{1}{2\pi}\int_{-\infty}^{\infty} \tilde{f}(x,y,\zeta)e^{jz\zeta}d\zeta \qquad (3.5)$$

$$\tilde{\tilde{f}}(\xi,y,\zeta) = \int_{-\infty}^{\infty} \tilde{f}(x,y,\zeta)e^{-jx\xi}dx \Leftrightarrow \tilde{f}(x,y,\zeta) = \frac{1}{2\pi}\int_{-\infty}^{\infty} \tilde{\tilde{f}}(\xi,y,\zeta)e^{jx\xi}d\xi \qquad (3.6)$$

Transforming the vector potential boundary conditions to the $\xi, \zeta$ domain leads to the following spectral representation of the vector potential boundary conditions,

$$\tilde{\tilde{A}}_x(\xi, y = \pm h, \zeta) = 0 \qquad (3.7)$$

$$\frac{\partial \tilde{\tilde{A}}_y(\xi, y = \pm h, \zeta)}{\partial y} = 0 \tag{3.8}$$

$$\tilde{\tilde{A}}_z(\xi, y = \pm h, \zeta) = 0 \tag{3.9}$$

As in equations (3.2)-(3.4), equations (3.7)-(3.9) indicate that the tangential components of the vector potential vanishes at the PEC boundary; similarly, the normal derivative of the normal component is also zero. These boundary conditions will be used to find the desired Green's function. The general solution to the vector potential wave equation is found next.

### *3.3 Solution of the Vector Potential Wave Equation*

A general solution to the vector potential wave equation,

$$\nabla^2 \vec{A}(x, y, z) + k^2 \vec{A}(x, y, z)) = -\mu \vec{J}(x, y, z), \tag{3.10}$$

can be found as the linear superposition of principal and reflected contributions. The principal contribution is related with a general current immersed in a homogenous space similar the the material found between the ground planes of the parallel plate waveguide. The reflected contribution is due to the presence of the ground planes. The respective contributions satisfy the differential equations given by

$$\nabla^2 A^p_\alpha(x, y, z) + k^2 A^p_\alpha(x, y, z) = -\mu J_\alpha(x, y, z) \ldots \alpha = x, y, z \tag{3.11}$$

$$\nabla^2 A^r_\alpha(x, y, z) + k^2 A^r_\alpha(x, y, z) = 0 \ldots \alpha = x, y, z \tag{3.12}$$

where the superscript $p$ denotes the principal contribution of the general wave equation and the superscript $r$ denotes the reflected contribution of the general wave equation. The total solution is

$$A_\alpha(x, y, z) = A^p_\alpha(x, y, z) + A^r_\alpha(x, y, z) \ldots \alpha = x, y, z \tag{3.13}$$

The solutions to the principle and the reflected parts are described in the sections that follow.

*3.3.1 Principal Solution.* The principal part of the vector potential wave equation(3.11) can be solved using a Fourier transform based complex-plane analysis. Transforming on $z$ and $x$ according to the transform pairs (3.5) and (3.6)(with the aid of the Fourier differentiation theorem) leads to

$$\frac{\partial^2 \tilde{\tilde{A}}^p_\alpha(\xi, y, \zeta)}{\partial y^2} - p^2 \tilde{\tilde{A}}^p_\alpha(x, y, z) = -\mu \tilde{\tilde{J}}_\alpha(\xi, y, \zeta) \ldots \alpha = x, y, z \tag{3.14}$$

where $p = \sqrt{\xi^2 + \zeta^2 - k^2}$. Note, $\xi$ is an $x$-directed wave number playing the role of $k_x$, $p$ is a $y$-directed wave number playing the role of $jk_y$ and $\zeta$ is a $z$-directed wave number playing the role of $k_z$.

Since $A^p_\alpha(x, y, z)$ is associated with a current in an unbounded region, a Fourier transform on $y$ can also be performed according to the definition below, namely

$$\tilde{\tilde{\tilde{f}}}(\xi, \eta, \zeta) = \int_{-\infty}^{\infty} \tilde{\tilde{f}}(\xi, y, \zeta) e^{-j\eta y} dy \Leftrightarrow \tilde{\tilde{f}}(\xi, y, \zeta) = \frac{1}{2\pi} \int_{-\infty}^{\infty} \tilde{\tilde{\tilde{f}}}(\xi, \eta, \zeta) e^{j\eta y} d\eta. \tag{3.15}$$

Completing the desired transform leads to

$$\begin{aligned} -(\eta^2 + p^2) \tilde{\tilde{\tilde{A}}}^p_\alpha(\xi, \eta, \zeta) &= -\mu \tilde{\tilde{\tilde{J}}}_\alpha(\xi, \eta, \zeta) \\ \tilde{\tilde{\tilde{A}}}^p_\alpha(\xi, \eta, \zeta) &= \frac{\mu \tilde{\tilde{\tilde{J}}}_\alpha(\xi, \eta, \zeta)}{(\eta^2 + p^2)} \\ &= \frac{\mu \tilde{\tilde{\tilde{J}}}_\alpha(\xi, \eta, \zeta)}{(\eta + jp)(\eta - jp)} \end{aligned} \tag{3.16}$$

Since boundary conditions will need to be enforced on the total solution at $y = \pm h$, an inverse Fourier transform must be performed on the principal contribution

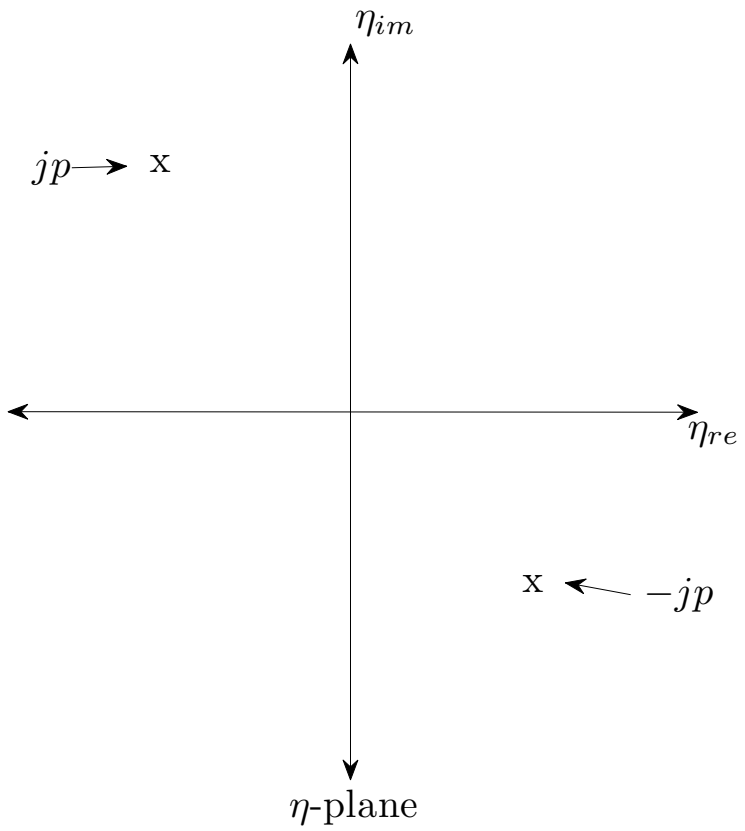


Figure 3.2: Singularities of the Integrand of Equation (3.17) in Complex $\eta$ Plane.

to return it to the $y$-domain. The inverse transform,

$$\tilde{\tilde{A}}^p_\alpha(\xi, y, \zeta) = \frac{1}{2\pi} \int_{-\infty}^{\infty} \tilde{\tilde{\tilde{A}}}^p_\alpha(\xi, \eta, \zeta) e^{j\eta y} d\eta = \frac{1}{2\pi} \int_{-\infty}^{\infty} \frac{\mu \tilde{\tilde{\tilde{J}}}_\alpha(\xi, \eta, \zeta)}{(\eta + jp)(\eta - jp)} e^{j\eta y} d\eta, \qquad (3.17)$$

is accomplished with the aid of complex analysis, as discussed next.

*3.3.1.1 Singularity Location and Closure Conditions.* For the integrand of equation (3.17), the only singularities are simple poles, $\eta = \pm jp$. The location of these poles can be determined by examining the expression $p = \sqrt{\xi^2 + \zeta^2 - k^2}$. Note, $\xi$ and $\zeta$ are the integration variables along the real axis and are purely real. Furthermore, for passive media $k$, given by $k = \omega\sqrt{\epsilon\mu}$, will have a positive real part and a negative imaginary part. Hence, $k^2$ will be found in the third and fourth quad-

rants of the complex plane. Likewise, $p^2$ ($p^2 \sim -k^2$) will be found in the first and second quadrants of the complex plane. Taking the root of $p^2$, $p$ and $-p$ will be found in the first and third quadrants of the complex plane respectively. Finally, the multiplication of the value of $p$ with $j$ will rotate the location of the pole into the second and forth quadrant of the complex $\eta$-plane (See Figure 3.2).

Cauchy's integral theorem can be used in the evaluation on the real-axis integral in equation (3.17). An appropriate contour for the case of $y > y'$ is shown in Figure 3.3. Note, since

$$e^{j\eta(y-y')} = e^{-\eta_{im}(y-y')} e^{j\eta_{re}(y-y')} \tag{3.18}$$

a careful inspection reveals that the following closure conditions must be obeyed for convergence [17]:

1. Case $y - y' > 0$: $e^{-\eta_{im}(y-y')}$ provides decay if $\eta_{im} > 0$ and an upper-half plane closure (UHPC) will ensure the infinite semi-circular contribution vanishes as $\eta$ approaches $\infty$.
2. Case $y - y' < 0$: $e^{-\eta_{im}(y-y')}$ provides decay if $\eta_{im} < 0$ and a lower-half plane closure (LHPC) is required to ensure the infinite semi-circular contribution vanishes as $\eta$ approaches $\infty$.

Thus, the relation of the observer location ($y$) to the source location ($y'$) determines whether an UHPC ($y > y'$) or a LHPC ($y < y'$) is required.

*3.3.1.2 Applying Cauchy Integral Formula.* Now that the singularities have been identified and the closure conditions investigated, we may now proceed in finding $\tilde{\tilde{A}}^p_\alpha(\xi, y, \zeta)$. Only the case of $y > y'$ will be presented here.

Recall that $\tilde{\tilde{\tilde{J}}}_\alpha(\xi, \eta, \zeta)$ can be written according to the following Fourier transform pair,

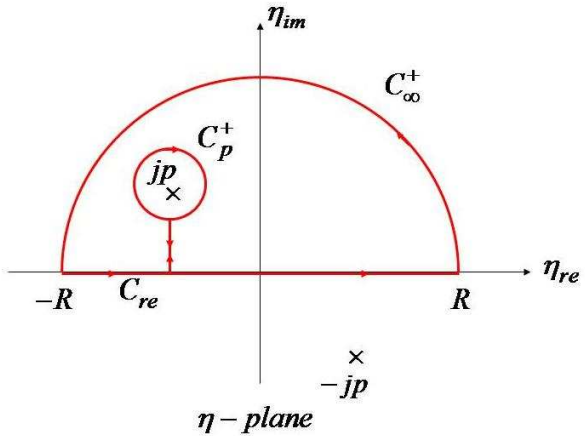


Figure 3.3: Upper-Half Plane Closure used to integrate case $y > y'$

$$\tilde{\tilde{J}}_\alpha(\xi,\eta,\zeta) = \int_{-\infty}^{\infty} \tilde{\tilde{J}}_\alpha(\xi,y',\zeta)e^{-j\eta y'}dy' = \int_{-h}^{h} \tilde{\tilde{J}}_\alpha(\xi,y',\zeta)e^{-j\eta y'}dy'. \tag{3.19}$$

Note, the region of existence of the current is physically confined within the parallel-plate background environment $-h < y < h$; accordingly, the limits of integration can be truncated to neglect the portions beyond the boundaries that don't contribute to the integral (i.e., $J_\alpha(x, h < y < \infty, z) = 0$)). Substituting (3.19) into (3.17) leads to

$$\begin{aligned}\tilde{\tilde{A}}_\alpha^p(\xi,y,\zeta) &= \frac{1}{2\pi}\int_{-\infty}^{\infty} \frac{\mu \int_{-h}^{h} \tilde{\tilde{J}}_\alpha(\xi,y',\zeta)e^{-j\eta y'}dy'}{(\eta+jp)(\eta-jp)}e^{j\eta y}d\eta \\ &= \int_{-h}^{h}\left(\frac{1}{2\pi}\int_{-\infty}^{\infty}\frac{e^{j\eta(y-y')}}{(\eta+jp)(\eta-jp)}d\eta\right)\mu\tilde{\tilde{J}}_\alpha(\xi,y',\zeta)dy' \end{aligned} \tag{3.20}$$

where

$$\tilde{\tilde{G}}_{\alpha\alpha}^p(\xi,\zeta;y-y') = \frac{1}{2\pi}\int_{-\infty}^{\infty}\frac{e^{j\eta(y-y')}}{(\eta+jp)(\eta-jp)}d\eta \tag{3.21}$$

is the spectral domain (i.e., the $\xi, \zeta$- domain) Green's function for the principal wave contribution.

A closed form expression for the spectral domains Green's function is calculated next using complex plane analysis. Only the process for the case $y > y'$ (UPHC) will be presented (see Figure 3.3). Momentarily neglecting the factor $\frac{1}{2\pi}$ in the spectral domain Green's function, the desired inverse Fourier transform integral to be calculated is

$$\begin{aligned}\int_{-\infty}^{\infty} \frac{e^{j\eta(y-y')}}{(\eta+jp)(\eta-jp)}d\eta &= \lim_{R\to\infty}\int_{C_{re}} \frac{e^{j\eta(y-y')}}{(\eta+jp)(\eta-jp)}d\eta \\ &= \lim_{R\to\infty}\int_{-R}^{R} \frac{e^{j\eta(y-y')}}{(\eta+jp)(\eta-jp)}d\eta \end{aligned} \tag{3.22}$$

Applying Cauchy's Integral Theorem [3] leads to

$$\begin{aligned}\lim_{R\to\infty} &\int_{-R}^{R} \frac{e^{j\eta(y-y')}}{(\eta+jp)(\eta-jp)}d\eta + \oint_{C_p^+} \frac{e^{j\eta(y-y')}}{(\eta+jp)(\eta-jp)}d\eta \\ &+ \lim_{R\to\infty}\int_{C_\infty^+} \frac{e^{j\eta(y-y')}}{(\eta+jp)(\eta-jp)}d\eta = 0 \end{aligned} \tag{3.23}$$

$$\begin{aligned}\lim_{R\to\infty} &\int_{-R}^{R} \frac{e^{j\eta(y-y')}}{(\eta+jp)(\eta-jp)}d\eta = \\ &- \oint_{C_p^+} \frac{e^{j\eta(y-y')}}{(\eta+jp)(\eta-jp)}d\eta - \lim_{R\to\infty}\int_{C_\infty^+} \frac{e^{j\eta(y-y')}}{(\eta+jp)(\eta-jp)}d\eta \end{aligned} \tag{3.24}$$

The left-hand side of equation (3.24) represents the desired integration along the real axis. The right-hand side of equation (3.24) is solved using Cauchy's integral formula

and Jordan's Lemma [3], leading to

$$-\oint_{C_p^+} \frac{e^{j\eta(y-y')}}{(\eta+jp)(\eta-jp)}d\eta = -\oint_{C_p^+} \frac{e^{j\eta(y-y')}/(\eta+jp)}{(\eta-jp)}d\eta$$
$$= -\left[-j2\pi \frac{e^{j\eta(y-y')}}{(\eta+jp)}\,|_{\eta=jp}\right] = \frac{\pi e^{-p(y-y')}}{p}. \tag{3.25}$$

It should be noted that the negative of the residue is used to compensate for the clockwise direction of integration. The infinite semicircular contribution ($C_\infty^+$) vanishes according to Jordan's lemma. Furthermore, application of Jordan's lemma can be extended to $y = y'$, as the integrand still converges as strongly as $\frac{1}{\eta^2}$ for large $\eta$.

The combined result of both cases $y > y'$ and $y < y'$ is (the factor of $1/2\pi$ again once again included)

$$\tilde{\tilde{G}}^p_{\alpha\alpha}(\xi,\zeta;y-y') = \frac{e^{-p|y-y'|}}{2p} \tag{3.26}$$

which leads to

$$\tilde{\tilde{A}}^p_\alpha = \int_{y^*} \frac{e^{-p|y-y'|}}{2p}\mu\tilde{\tilde{J}}_\alpha dy' = \int_{-h}^{h} \frac{e^{-p|y-y'|}}{2p}\mu\tilde{\tilde{J}}_\alpha dy' \tag{3.27}$$

*3.3.2 Reflected Solution.* The form of the reflected portion of the vector wave equation in the $\xi,\zeta$-domain is easily determined

$$\frac{\partial^2 \tilde{\tilde{A}}^r_\alpha(\xi,y,\zeta)}{\partial y^2} - p^2\tilde{\tilde{A}}^r_\alpha(\xi,y,\zeta) = 0 \ldots \alpha = x,y,z. \tag{3.28}$$

Its harmonic solution is readily recognized to be, $\tilde{\tilde{A}}^r_\alpha = W^+_\alpha e^{-py} + W^-_\alpha e^{py}$. Note, the first term represents an up-going wave with complex amplitude $W^+_\alpha$ and the second term represents a down-going wave with complex amplitude $W^-_\alpha$.

## *3.4 Applying Boundary conditions to Total Solution*

Applying the boundary conditions; (3.7)-(3.9) to the total solution, $\tilde{\tilde{A}}_\alpha = \tilde{\tilde{A}}^p_\alpha + \tilde{\tilde{A}}^r_\alpha$, at $y = \pm h$ yields

$$\begin{aligned}\tilde{\tilde{A}}_\alpha &= \int_{y'} \frac{e^{-p|y-y'|}}{2p}\mu\tilde{\tilde{J}}dy' + \\ &\int_{y'} \left[\frac{\bar{R}_{\alpha\alpha}e^{-p(y'+2h+y)} + \bar{R}_{\alpha\alpha}\bar{\bar{R}}_{\alpha\alpha}e^{-p(-y'+4h+y)}}{2p(1-\bar{R}_{\alpha\alpha}\bar{\bar{R}}_{\alpha\alpha}e^{-4ph})}\right. \\ &\left. + \frac{\bar{\bar{R}}_{\alpha\alpha}e^{-p(-y'+2h-y)} + \bar{R}_{\alpha\alpha}\bar{\bar{R}}_{\alpha\alpha}e^{-p(y'+4h-y}}{2p(1-\bar{R}_{\alpha\alpha}\bar{\bar{R}}_{\alpha\alpha}e^{-4ph})}\right]\mu\tilde{\tilde{J}}_\alpha dy' \end{aligned} \tag{3.29}$$

where $\bar{R}_{\alpha\alpha}$ is the reflection coefficient for the lower ground plane, $\bar{\bar{R}}_{\alpha\alpha}$ is the reflection coefficient for the upper ground plane and $p = \sqrt{\xi^2 + \zeta^2 - k^2}$. All of the integrand in equation(3.29) being multiplied by $\mu\tilde{\tilde{J}}$ represents the vector potential parallel-plate Green's function in the spectral $(\xi, \zeta)$ domain.

In this form (3.29), a great deal of physical meaning can be gleaned. As seen in Figure 3.4, each term in the solution accounts for a different possible path from the source, $y'$ ,to the observer, $y$ [17].

- The 1st path, direct from source to observe, is accounted for in the contribution from the principal part, $e^{-p(y-y')}$
- The 2nd path, from the source to the observe after reflection off the upper-conductor, is accounted for in the term $\bar{\bar{R}}e^{-p(-y'+2h-y)}$
- The 3rd path, from the source to the observer after reflection off the lower-conductor, is accounted for in the term $\bar{R}e^{-p(y'+2h+y)}$
- The 4th path, from the source off the top-conductor, then the bottom-conductor then to the source, is accounted for in the term $\bar{R}\bar{\bar{R}}e^{-p(-y'+4h+y)}$
- The final path, the inverse of the 4th path, is accounted for in the 5th term $\bar{R}\bar{\bar{R}}e^{-p(y'+4h-y)}$

Clearly, the proposed principal contribution is related to the forced response in unbounded media while the reflected contribution accounts for the reflected response.

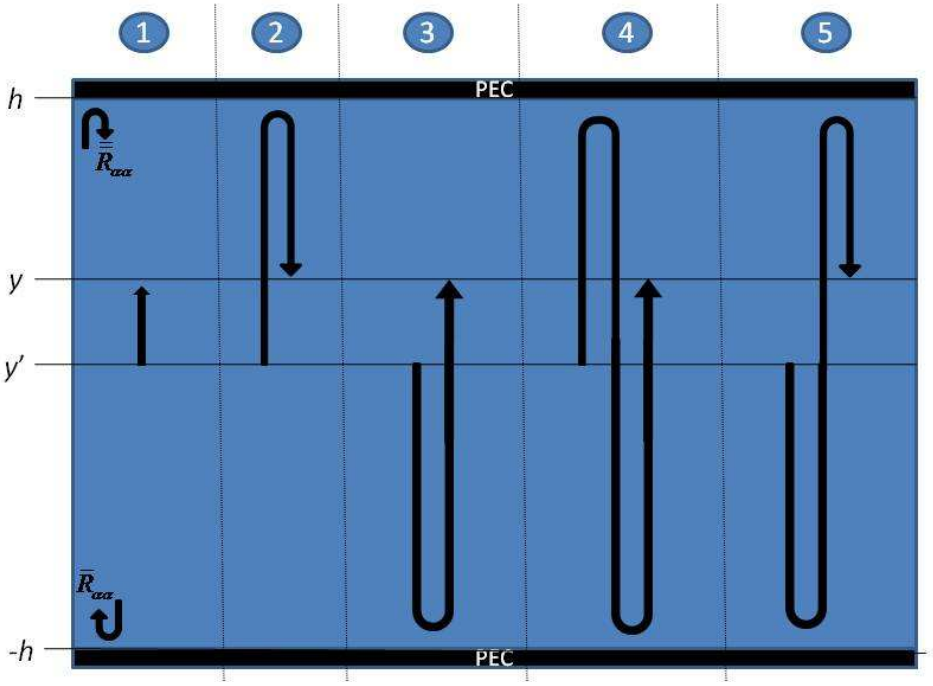


Figure 3.4: Each Possible path (1-5) from the source to the observer is accounted for in equation (3.29).

A more compact version of the Green's function can be found by using the definition of hyperbolic functions and setting $\bar{R}_{\alpha\alpha}, \bar{\bar{R}}_{\alpha\alpha} = -1 \ldots \alpha = x, z, \bar{R}_{yy}, \bar{\bar{R}}_{yy} = 1$. Equation (3.29) reduces to

$$\tilde{\tilde{G}}_{\alpha\alpha}(\xi, \zeta; y \mid y_o) = \begin{cases} \frac{cosh[p(2h-|y-y'|)]-cosh[p(y+y')]}{2psinh(2ph)} & \text{if } \alpha = x, z, \\ \frac{cosh[p(2h-|y-y'|)]+cosh[p(y+y')]}{2psinh(2ph)} & \text{if } \alpha = y. \end{cases} \tag{3.30}$$

Note, the Green's function is even in $p$, thus the square root branch cut contribution is removable, as physically expected for this closed structure.

### *3.5 Summary*

In this chapter, the vector potential parallel-plate Green's function for an electric current was developed. First, spectral and spacial vector potential boundary conditions for the parallel-plate wave guide were found. The forced vector potential wave equation was solved by decomposing the equation into principle and reflective parts. Each part was then solved independently. Complex analysis was used to find the solution to the principle part and the reflected part was readily identified as having a harmonic solution. Boundary conditions were applied to the total solution at the outer conductors to find the Green's function. The hyperbolic version of the Green's function (3.30) was identified and will be used in the next chapter to formulate an integral equation for a stripline.

# IV. Electric Field Integral Equations

## *4.1 Introduction*

In chapter 3, we discussed the development of the parallel-plate Green's function. In this chapter, we will use this Green's function to formulate coupled integral equations for finding the current on the center conductor of a stripline modeled as a strip embedded in a parallel-plate waveguide environment. First, a set of coupled integral equations will be formulated for a strip with infinite conductivity. This method will include converting the PEC boundary condition to the $\zeta$-domain (prompted by the infinite length along the $z$-axis). Finally, a specialized integral equation for a stripline supporting a TEM mode will be considered. In the next chapter, the method of moments will be used to solve for the unknown currents and guided propagation constant found in these integral equations.

## *4.2 Integral Equation Formulation for PEC Stripline*

The goal of this section is to formulate an integral equation for the unknown current density on the PEC center conductor of the stripline. Specifically, an electric field integral equation (EFIE) is developed by enforcing the well-known boundary condition

$$\hat{t} \cdot \vec{E} = 0 \ldots \hat{t} = \hat{x}, \hat{z} \tag{4.1}$$

on the PEC center strip. Note, it will be assumed that the PEC center strip is infinitesimally thin and located at $y = y_0$.

Decomposing the electric field in (4.1) into incident and scattered contributions, $\vec{E} = \vec{E}^i + \vec{E}^s$, leads to the result (for $\hat{t} = \hat{x}, \hat{z}$)

$$\hat{t} \cdot \vec{E}^s = -\hat{t} \cdot \vec{E}^i \quad or \quad E_x^s = -E_x^i, \quad E_z^s = -E_z^i \tag{4.2}$$

where

$$\vec{E}^s = \frac{1}{j\omega\epsilon\mu}(k^2 + \nabla\nabla\cdot)\vec{A}^s. \tag{4.3}$$

Substituting equation (4.3) into the leftside of the equation (4.2) and transforming to the $\zeta$-domain yields

$$\hat{t} \cdot \frac{1}{j\omega\epsilon\mu}(k^2 + \tilde{\nabla}\tilde{\nabla}\cdot)\tilde{\vec{A}}^s = -\hat{t} \cdot \vec{E}^i \ldots \hat{t} = \hat{x}, \hat{z} \tag{4.4}$$

where

$$\begin{aligned} \tilde{\nabla} &= \hat{x}\frac{\partial}{\partial x} + \hat{y}\frac{\partial}{\partial y} + j\zeta\hat{z} \\ \tilde{\vec{A}}^s &= \int_{y^*}\int_{x^*} \tilde{\bar{\bar{G}}}(\zeta; \vec{\rho} \mid \vec{\rho'}) \cdot \tilde{\vec{J}}(\rho', \zeta) dx' dy' \ldots \rho = x\hat{x} + y\hat{y} \ldots \rho' = x'\hat{x} + y'\hat{y}, \end{aligned} \tag{4.5}$$

$\tilde{\bar{\bar{G}}}(\rho \mid \rho', \zeta)$ is the $\zeta$-domain dyadic Green's function, $y^*, x^*$ is shorthand notation for the region of integration and $\tilde{\vec{J}}$, the $\zeta$-domain representation of a the $\ell^{th}$ natural mode z-propagating surface current on an infinitesimally thin center conductor, can be written as [28]

$$\tilde{\vec{J}} = \hat{x}\frac{\tilde{J}_{sx}(x)\delta(y - y_0)}{(\zeta - \zeta_\ell)} + \hat{z}\frac{\tilde{J}_{sz}(x)\delta(y - y_0)}{(\zeta - \zeta_\ell)}. \tag{4.6}$$

Additionally, the limits of integration for equation (4.5) can be reduced to the region where the strip exists ($-a < x' < a$).

Substituting equations (4.5) and (4.6) into equation (4.4) yields the following boundary condition relation for the $x$ and $z$ components of the electric field

$$
\begin{aligned}
&\frac{1}{j\omega\epsilon\mu}(k^2\tilde{A}_x + \frac{\partial^2}{\partial x^2}\tilde{A}_x + \frac{\partial}{\partial x}j\zeta\tilde{A}_z) = -\tilde{E}_x^i \\
&\frac{1}{j\omega\epsilon\mu}\left[\frac{\mu k^2}{2\pi}\int_{-a}^{a}\int_{-\infty}^{\infty}\tilde{\tilde{G}}_{xx}(\xi,\zeta;y_o \mid y_o)e^{jx\xi}e^{-jx'\xi}\frac{\tilde{J}_{sx}(x')}{(\zeta-\zeta_\ell)}d\xi dx'\right. \\
&\qquad -\frac{\mu}{2\pi}\int_{-a}^{a}\int_{-\infty}^{\infty}\xi^2\tilde{\tilde{G}}_{xx}(\xi,\zeta;y_o \mid y_o)e^{jx\xi}e^{-jx'\xi}\frac{\tilde{J}_{sx}(x')}{(\zeta-\zeta_\ell)}d\xi dx' \\
&\qquad \left.-\frac{\mu\zeta}{2\pi}\int_{-a}^{a}\int_{-\infty}^{\infty}\xi\tilde{\tilde{G}}_{zz}(\xi,\zeta;y_o \mid y_o)e^{jx\xi}e^{-jx'\xi}\frac{\tilde{J}_{sz}(x')}{(\zeta-\zeta_\ell)}d\xi dx'\right] = -\tilde{E}_x^i \\
&\int_{-a}^{a}\int_{-\infty}^{\infty}(k^2-\xi^2)\tilde{\tilde{G}}_{xx}(\xi,\zeta;y_o \mid y_o)e^{jx\xi}e^{-jx'\xi}\tilde{J}_{sx}(x')d\xi dx' \\
&\qquad -\int_{-a}^{a}\int_{-\infty}^{\infty}\zeta\xi\tilde{\tilde{G}}_{zz}(\xi,\zeta;y_o \mid y_o)e^{jx\xi}e^{-jx'\xi}\tilde{J}_{sz}(x')d\xi dx' \\
&\qquad = -2\pi j\omega\epsilon(\zeta-\zeta_\ell)\tilde{E}_x^i
\end{aligned}
\tag{4.7}
$$

$$\frac{1}{j\omega\epsilon\mu}(k^2\tilde{A}_z + \frac{\partial}{\partial x}j\zeta\tilde{A}_x - \zeta^2\tilde{A}_z)) = -\tilde{E}_z^i$$

$$\frac{1}{j\omega\epsilon\mu}\left[\frac{\mu k^2}{2\pi}\int_{-a}^{a}\int_{-\infty}^{\infty}\tilde{\tilde{G}}_{zz}(\xi,\zeta;y_o \mid y_o)e^{jx\xi}e^{-jx'\xi}\frac{\tilde{J}_{sz}(x')}{(\zeta-\zeta_\ell)}d\xi dx'\right.$$

$$-\frac{\mu}{2\pi}\int_{-a}^{a}\int_{-\infty}^{\infty}\xi\zeta\tilde{\tilde{G}}_{xx}(\xi,\zeta;y_o \mid y_o)e^{jx\xi}e^{-jx\xi}\frac{\tilde{J}_{sx}(x')}{(\zeta-\zeta_\ell)}d\xi dx'$$

$$\left.-\frac{\mu}{2\pi}\int_{-a}^{a}\int_{-\infty}^{\infty}\zeta^2\tilde{\tilde{G}}_{zz}(\xi,\zeta;y_o \mid y_o)e^{jx\xi}e^{-jx\xi}\frac{\tilde{J}_{sz}(x')}{(\zeta-\zeta_\ell)}d\xi dx'\right] = -\tilde{E}_z^i$$

$$-\int_{-a}^{a}\int_{-\infty}^{\infty}\zeta\xi\tilde{\tilde{G}}_{xx}(\xi,\zeta;y_o \mid y_o)e^{jx\xi}e^{-jx\xi}\tilde{J}_{sx}(x')d\xi dx'$$

$$+\int_{-a}^{a}\int_{-\infty}^{\infty}(k^2-\zeta^2)\tilde{\tilde{G}}_{zz}(\xi,\zeta;y_o \mid y_o)e^{jx\xi}e^{-jx\xi}\tilde{J}_{sz}(x')d\xi dx'$$

$$= -2\pi j\omega\epsilon(\zeta-\zeta_\ell)\tilde{E}_z^i \tag{4.8}$$

For natural mode propagation ($\zeta = \zeta_\ell$), of which the TEM is dominant, the right-hand side of equations (4.7) and (4.8) vanish [28] leading to the desired coupled EFIE's for the unknown currents $\tilde{J}_{sx}$ and $\tilde{J}_{sz}$, that is

$$\int_{-a}^{a}\int_{-\infty}^{\infty}(k^2-\xi^2)\tilde{\tilde{G}}_{xx}(\xi,\zeta;y_o\mid y_o)e^{jx\xi}e^{-jx'\xi}\tilde{J}_{sx}(x')d\xi dx'$$
$$-\int_{-a}^{a}\int_{-\infty}^{\infty}\zeta\xi\tilde{\tilde{G}}_{zz}(\xi,\zeta;y_o\mid y_o)e^{jx\xi}e^{-jx'\xi}\tilde{J}_{sz}(x')d\xi dx'=0 \tag{4.9}$$
$$-\int_{-a}^{a}\int_{-\infty}^{\infty}\zeta\xi\tilde{\tilde{G}}_{xx}(\xi,\zeta;y_o\mid y_o)e^{jx\xi}e^{-jx\xi}\tilde{J}_{sx}(x')d\xi dx'$$
$$+\int_{-a}^{a}\int_{-\infty}^{\infty}(k^2-\zeta^2)\tilde{\tilde{G}}_{zz}(\xi,\zeta;y_o\mid y_o)e^{jx\xi}e^{-jx\xi}\tilde{J}_{sz}(x')d\xi dx'=0 \tag{4.10}$$

It should be noted that the first integral in equation (4.9) accounts for the $x$ component of the scattered electric field maintained by the $x$ component of current. The second integral in of equation (4.9) accounts for the $x$ component of the scattered electric field maintained by the $z$ component of current. The first integral in equation (4.10) accounts for the $z$ component of the scattered electric field maintained by the $x$ component of current. Finally, the last line in integral (4.10) accounts for the $z$ component of the scattered electric field maintained by the $z$ component of the current. These relationships will be exploited in the next section to find a specialized TEM integral equation and will subsequently lead to enhanced computational efficiency.

### *4.3 TEM Specialization of a PEC Stripline*

For TEM mode propagation in the air filled, lossless stripline, there is no $x$ component of the current , that is, $\tilde{J}_{sx}=0$ and the propagation constant takes on the value $\zeta=k=k_0$ (see Section 5.3 for more information on these results). Under these circumstances, equation (4.10) vanishes and equation (4.9) reduces to

$$\int_{-a}^{a}\int_{-\infty}^{\infty}k_0\xi\tilde{\tilde{G}}_{zz}(\xi,k_0;y_o\mid y_o)e^{jx\xi}e^{-jx'\xi}\tilde{J}_{sz}(x')d\xi dx'=0 \tag{4.11}$$

Equation (4.11) represents a single EFIE for the unknown surface current $\tilde{J}_{sz}$ of the Dominant TEM mode, and will be explored in the next chapter. It is anticipated that substantial computational gains will be achieved, compared to the coupled EFIE equations (4.9) and (4.10). Note, if the properties of higher order modes are sought, the coupled EFIE must be used.

## *4.4 Summary*

In this chapter, coupled integral equations were formulated for a stripline having a perfect center conductor. Furthermore, it was shown that the coupled integral equation reduce to a single integral equation for the TEM mode. This specialization naturally leads to a more computationally efficient formulation. The solution of these integral equations will be sought in the following chapter.

# V. Method of Moments

## *5.1 Introduction*

In this chapter, an efficient entire-domain method of moments (MoM) technique will be used to solve the integral equations formulated in the last chapter. For the coupled integral equations formulated for the perfectly conducting center conductor, a Galerkin's based MoM is found with the aid of Chebyshev polynomials. Solutions will be found for both the general coupled EFIE formulation and the specialized TEM EFIE formulation. The currents ($\tilde{J}_{sx}$ and $\tilde{J}_{sz}$) and guided propagation constant ($\zeta$) found for each of these formulations through this process will be used in the next chapter to calculate the desired characteristic impedance of the stripline.

## *5.2 MoM Solution of Coupled EFIE's for PEC Strip*

In this section, a Galerkin's based MoM solution is sought for the coupled EFIE's for the stripline having a PEC center strip. Two different scenarios of test and expansion functions will be investigated. It will be shown that the second set of expansion and testing functions has more desirable rates of convergence, and will therefore be used in solving for the unknown currents and calculation of the characteristic impedance and TEM mode propagation constant.

*5.2.1 General MoM Solution.* In the previous chapter, it was shown that the coupled integral equation (CIE) for a stripline having a PEC center conductor are given by

$$\int_{-a}^{a}\int_{-\infty}^{\infty}(k^2-\xi^2)\tilde{\tilde{G}}_{xx}(\xi,\zeta;y_o|y_o)e^{jx\xi}e^{-jx'\xi}\tilde{J}_{sx}(x')d\xi dx' - \int_{-a}^{a}\int_{-\infty}^{\infty}\xi\zeta\tilde{\tilde{G}}_{zz}(\xi,\zeta;y_o|y_o)e^{jx\xi}e^{-jx'\xi}\tilde{J}_{sz}(x')d\xi dx' = 0 \tag{5.1}$$

$$-\int_{-a}^{a}\int_{-\infty}^{\infty}\xi\zeta\tilde{\tilde{G}}_{xx}(\xi,\zeta;y_o|y_o)e^{jx\xi}e^{-jx'\xi}\tilde{J}_{sx}(x')d\xi dx' + \int_{-a}^{a}\int_{-\infty}^{\infty}(k^2-\zeta^2)\tilde{\tilde{G}}_{zz}(\xi,\zeta;y_o|y_o)e^{jx\xi}e^{-jx'\xi}\tilde{J}_{sz}(x')d\xi dx' = 0. \tag{5.2}$$

The first step in the MoM solution is to expand the unknown currents $\tilde{J}_{sx}, \tilde{J}_{sz}$ according to the weighted sum given by

$$\tilde{J}_{s\alpha}(x') = \sum_{n=0}^{N-1} a_{n\alpha}e_{n\alpha}(x')\ldots\alpha = x, z \tag{5.3}$$

where $e_{n\alpha}(x')$ are known expansion functions and $a_{n\alpha}$ are unknown expansion coefficients. Substituting (5.3) into (5.1) and (5.2) leads to

$$\sum_{n=0}^{N-1}a_{nx}\int_{-\infty}^{\infty}(k^2-\xi^2)\tilde{\tilde{G}}_{xx}(\xi,\zeta;y_o|y_o)e^{jx\xi}\int_{-a}^{a}e_{nx}(x')e^{-jx'\xi}dx'd\xi - \sum_{n=0}^{N-1}a_{nz}\int_{-\infty}^{\infty}\xi\zeta\tilde{\tilde{G}}_{zz}(\xi,\zeta;y_o|y_o)e^{jx\xi}\int_{-a}^{a}e_{nz}(x')e^{-jx'\xi}dx'd\xi = 0 \tag{5.4}$$

$$-\sum_{n=0}^{N-1}a_{nx}\int_{-\infty}^{\infty}\xi\zeta\tilde{\tilde{G}}_{xx}(\xi,\zeta;y_o|y_o)e^{jx\xi}\int_{-a}^{a}e_{nx}(x')e^{-jx'\xi}dx'd\xi + \sum_{n=0}^{N-1}a_{nz}\int_{-\infty}^{\infty}(k^2-\zeta^2)\tilde{\tilde{G}}_{zz}(\xi,\zeta;y_o|y_o)e^{jx\xi}\int_{-a}^{a}e_{nz}(x')e^{-jx'\xi}dx'd\xi = 0. \tag{5.5}$$

Defining $g_{n\alpha}(\xi)$ as

$$g_{n\alpha}(\xi) = \int_{-a}^{a}e_{n\alpha}(x')e^{-jx'\xi}dx'\ldots\alpha = x, z \tag{5.6}$$

allows (5.4) and (5.5) to be simplified as follows

$$\sum_{n=0}^{N-1} a_{nx} \int_{-\infty}^{\infty} (k^2 - \xi^2) \tilde{\tilde{G}}_{xx}(\xi, \zeta; y_o|y_o) e^{jx\xi} g_{nx}(\xi) d\xi$$
$$- \sum_{n=0}^{N-1} a_{nz} \int_{-\infty}^{\infty} \xi\zeta \tilde{\tilde{G}}_{zz}(\xi, \zeta; y_o|y_o) e^{jx\xi} g_{nz}(\xi) d\xi = 0 \tag{5.7}$$

$$- \sum_{n=0}^{N-1} a_{nx} \int_{-\infty}^{\infty} \xi\zeta \tilde{\tilde{G}}_{xx}(\xi, \zeta; y_o|y_o) e^{jx\xi} g_{nx}(\xi) d\xi$$
$$+ \sum_{n=0}^{N-1} a_{nz} \int_{-\infty}^{\infty} (k^2 - \zeta^2) \tilde{\tilde{G}}_{zz}(\xi, \zeta; y_o|y_o) e^{jx\xi} g_{nz}(\xi) d\xi = 0. \tag{5.8}$$

Equations (5.7) and (5.8) represent 2 equations and $2N$ unknowns. In order to establish a $2N \times 2N$ MoM matrix, the following testing operators are applied as the next step in the MoM solution, namely

$$\int_{-a}^{a} [\quad] t_{m\alpha}(x) dx \ldots \alpha = x, z \quad and \quad m = 0, \ldots, N-1 \tag{5.9}$$

where $t_{m\alpha}(x)$ is a known testing function. Applying the $\alpha = x$ testing operator to (5.7), the $\alpha = z$ testing operator to (5.8) and defining $f_{m\alpha}(\xi)$ as

$$f_{m\alpha}(\xi) = \int_{-a}^{a} t_{m\alpha}(x) e^{jx\xi} dx \tag{5.10}$$

results in the following coupled equation

$$\sum_{n=0}^{N-1} a_{nx} \int_{-\infty}^{\infty} (k^2 - \xi^2) \tilde{\tilde{G}}_{xx}(\xi, \zeta; y_o|y_o) f_{mx}(\xi) g_{nx}(\xi) d\xi$$
$$- \sum_{n=0}^{N-1} a_{nz} \int_{-\infty}^{\infty} \xi\zeta \tilde{\tilde{G}}_{zz}(\xi, \zeta; y_o|y_o) f_{mx}(\xi) g_{nz}(\xi) d\xi = 0 \ldots m = 0, \ldots, N-1 \tag{5.11}$$

$$-\sum_{n=0}^{N-1} a_{nz} \int_{-\infty}^{\infty} \xi\zeta \tilde{\tilde{G}}_{xx}(\xi, \zeta; y_o|y_o) f_{mz}(\xi) g_{nx}(\xi) d\xi$$
$$+ \sum_{n=0}^{N-1} a_{nz} \int_{-\infty}^{\infty} (k^2 - \zeta^2) \tilde{\tilde{G}}_{zz}(\xi, \zeta; y_o|y_o) f_{mz}(\xi) g_{nz}(\xi) d\xi = 0 \ldots m = 0, \ldots, N-1 \tag{5.12}$$

which can be further simplified as

$$\begin{aligned} \sum_{n=0}^{N} a_{nx} A_{xx}^{mn} \quad + \quad \sum_{n=0}^{N} a_{nz} A_{xz}^{mn} = 0 \ldots m = 0, \ldots, N-1 \\ \sum_{n=0}^{N} a_{nx} A_{zx}^{mn} \quad + \quad \sum_{n=0}^{N} a_{nz} A_{zz}^{mn} = 0 \ldots m = 0, \ldots, N-1 \end{aligned} \tag{5.13}$$

where

$$A_{xx}^{mn} = \int_{-\infty}^{\infty} (k^2 - \xi^2) \tilde{\tilde{G}}_{xx}(\xi, \zeta; y_o|y_o) f_{mx}(\xi) g_{nx}(\xi) d\xi \tag{5.14}$$

$$A_{zx}^{mn} = -\int_{-\infty}^{\infty} \xi\zeta \tilde{\tilde{G}}_{zz}(\xi, \zeta; y_o|y_o) f_{mx}(\xi) g_{nz}(\xi) d\xi \tag{5.15}$$

$$A_{xz}^{mn} = -\int_{-\infty}^{\infty} \xi\zeta \tilde{\tilde{G}}_{xx}(\xi, \zeta; y_o|y_o) f_{mz}(\xi) g_{nz}(\xi) d\xi \tag{5.16}$$

$$A_{zz}^{mn} = \int_{-\infty}^{\infty} (k^2 - \zeta^2) \tilde{\tilde{G}}_{zz}(\xi, \zeta; y_o|y_o) f_{mz}(\xi) g_{nz}(\xi) d\xi. \tag{5.17}$$

Note, $A_{\alpha\beta}^{mn}$ (with $\alpha$ and $\beta$ equal to $x, z$) physically represents how the $n^{th}$ $\beta$-directed source current term couples into the $m^{th}$ $\alpha$-directed field term. Next, two specific scenarios of expansion and testing functions will be investigated.

*5.2.2 Galerkin Method Using Chebsyshev Polynomials of the First Kind.*

Selecting the "best" expansion/testing functions has been shown to improve the accuracy and computational efficiency of the MoM [4, 5, 19, 29]. Using an entire-domain technique can further improve efficiency because fewer terms are required in the expansion leading to a smaller MoM matrix [5]. Chebsyshev polynomials make excellent expansion and testing functions in this research because of their ability to model current behavior on a strip, include edge effects [4, 14]. The proposed testing and expansion functions in the first scenario are given by [17]

$$t_{nx} = e_{nx} = T_{(2n+1)}(\frac{x}{a})\sqrt{1-(\frac{x}{a})^2}...(\text{odd function}) \tag{5.18}$$

$$t_{nz} = e_{nz} = \frac{T_{(2n)}(\frac{x}{a})}{\sqrt{1-(\frac{x}{a})^2}}...(\text{even function}) \tag{5.19}$$

This choice is prompted by the dominant TEM mode behavior characterized by an even longitudinal current and an odd transverse current [17]. An additional advantage of this selection is that a closed form solution for $f_{m\alpha}(\xi)$ and $g_{n\alpha}(\xi)$, which are given by

$$f_{m\alpha}(\xi) = \begin{cases} \int_{-a}^{a} T_{2m+1}(\frac{x}{a})\sqrt{1-(\frac{x}{a})^2}e^{jx\xi}dx & \text{if } \alpha = x \\ \int_{-a}^{a} \frac{T_{2m}(\frac{x}{a})}{\sqrt{1-(\frac{x}{a})^2}}e^{jx\xi}dx & \text{if } \alpha = z \end{cases} \tag{5.20}$$

and

$$g_{n\alpha}(\xi) = \begin{cases} \int_{-a}^{a} T_{2n+1}(\frac{x}{a})\sqrt{1-(\frac{x}{a})^2}e^{-jx\xi}dx & \text{if } \alpha = x \\ \int_{-a}^{a} \frac{T_{2n}(\frac{x}{a})}{\sqrt{1-(\frac{x}{a})^2}}e^{-jx\xi}dx & \text{if } \alpha = z \end{cases} \tag{5.21}$$

can be found [17]. Substitution of(5.20) and (5.21) into (5.14)-(5.17) leads to

$$A_{xx}^{mn} = \frac{a}{(-j)^{2n}} \int_{-\infty}^{\infty} (k^2 - \xi^2)\tilde{\tilde{G}}_{xx}(\xi, \zeta; y_o|y_o)[J_{2m+1}(a\xi) + \frac{1}{2}(J_{2m+3}(a\xi) + J_{2m-1}(a\xi))]$$
$$[J_{2n+1}(a\xi) + \frac{1}{2}(J_{2n+3}(a\xi) + J_{2n-1}(a\xi))]d\xi \tag{5.22}$$
$$A_{xz}^{mn} = -j(-1)^n \int_{-\infty}^{\infty} \xi\zeta\tilde{\tilde{G}}_{zz}(\xi, \zeta; y_o|y_o)[J_{2m+1}(a\xi) + \frac{1}{2}(J_{2m+3}(a\xi) + J_{2m-1}(a\xi))]$$
$$J_{2n}(a\xi)d\xi \tag{5.23}$$
$$A_{zx}^{mn} = \frac{ja}{(-j)^{2n}} \int_{\infty}^{\infty} -\xi\zeta\tilde{\tilde{G}}_{xx}(\xi, \zeta; y_o|y_o)J_{2m}(a\xi)$$
$$[J_{2n+1}(a\xi) + \frac{1}{2}(J_{2n+3}(a\xi) + J_{2n-1}(a\xi))]d\xi \tag{5.24}$$
$$A_{zz}^{mn} = (-1)^n \int_{-\infty}^{\infty} (k^2 - \zeta^2)\tilde{\tilde{G}}_{zz}(\xi, \zeta; y_o|y_o)J_{2m}(a\xi)J_{2n}(a\xi)d\xi, \tag{5.25}$$

where $J_n$ is a Bessel Function of the $n^{th}$ order. Since the integrals in (5.22)-(5.25) involve infinite limits, it is important to understand the asymptotic behavior of these integrands to address the issue of convergence. Using the large argument approximation of the Bessel function in conjunction with the large argument behavior of the Green's function, given by

$$G_{\alpha\alpha} \sim \frac{1}{\xi} \quad \forall \quad \alpha = x, z \quad \xi \to \infty, \tag{5.26}$$

the asymptotic behavior of the integrands are found to be

$$I(A_{xx}^{mn}) \sim 0 \tag{5.27}$$
$$I(A_{zx}^{mn}) \sim \frac{1}{\xi} \tag{5.28}$$
$$I(A_{xz}^{mn}) \sim \frac{1}{\xi} \tag{5.29}$$
$$I(A_{zz}^{mn}) \sim \frac{1}{\xi^2} \tag{5.30}$$

where $I(A_{\alpha\beta}^{mn})$ is the integrand of the integral corresponding to $A_{\alpha\beta}^{mn}$. Note, the desired computational efficiency cannot be achieved due to the slow convergence (less than $\frac{1}{\xi^2}$), thus a more suitable expansion/test set will be studied in the next section.

### *5.2.3 Galerkin Method Using Chebsyshev Polynomials of the First/Second Kind.*

Improved convergence can be achieved by selecting a more suitable expansion/testing function set. The following expansion and test functions were selected [17]:

$$t_{nx} = e_{nx} = U_{(2n+1)}(\frac{x}{a})\sqrt{1-(\frac{x}{a})^2}...(\text{odd function}) \tag{5.31}$$

$$t_{nz} = e_{nz} = \frac{T_{(2n)}(\frac{x}{a})}{\sqrt{1-(\frac{x}{a})^2}}...(\text{even function}) \tag{5.32}$$

to improve computational efficiency while maintaining the ability to model current behavior. New values of $f_{mz}$ and $g_{nz}$, must be calculated and are discussed next.

#### *5.2.3.1 Evaluation of $f_{mz}$ and $g_{nz}$.*

Applying equation (5.32) to the definition of $f_{mz}$ and $g_{nz}$ yields

$$\begin{aligned} f_{mz}(\xi) &= \int_{-a}^{a} \frac{T_{(2m)}(\frac{x}{a})}{\sqrt{1-(\frac{x}{a})^2}} e^{jx\xi} dx \\ &= \int_{-a}^{a} \frac{T_{(2m)}(\frac{x}{a})}{\sqrt{1-(\frac{x}{a})^2}} \cos(x\xi)dx + \underbrace{j\int_{-a}^{a} \frac{T_{(2m)}(\frac{x}{a})}{\sqrt{1-(\frac{x}{a})^2}} \sin(x\xi)dx}_{=0} ...\text{c.o.v } \tilde{x} = \frac{x}{a} \\ &= 2a\int_{0}^{1} \frac{T_{(2m)}(\tilde{x})}{\sqrt{1-(\tilde{x})^2}} \cos(a\tilde{x}\xi)d\tilde{x} \\ &= 2aI_{fmz}^{e}(a\xi) \end{aligned} \tag{5.33}$$

and

$$\begin{aligned} g_{nz}(\xi) &= \int_{-a}^{a} \frac{T_{(2n)}(\frac{x}{a})}{\sqrt{1-(\frac{x}{a})^2}} e^{-jx\xi} dx \\ &= \int_{-a}^{a} \frac{T_{(2n)}(\frac{x}{a})}{\sqrt{1-(\frac{x}{a})^2}} \cos(x\xi) dx - \underbrace{j \int_{-a}^{a} \frac{T_{(2n)}(\frac{x}{a})}{\sqrt{1-(\frac{x}{a})^2}} \sin(x\xi) dx}_{=0} \text{ ...c.o.v } \tilde{x} = \frac{x}{a} \\ &= 2a \int_{0}^{1} \frac{T_{(2n)}(\tilde{x})}{\sqrt{1-(\tilde{x})^2}} \cos(a\tilde{x}\xi) d\tilde{x} \\ &= 2aI^{e}_{gnz}(a\xi) \end{aligned} \tag{5.34}$$

where (see Appendix A)

$$I^{e}_{fmz}(a\xi) = I^{e}_{gnz}(a\xi) = \begin{cases} (-1)^n (\frac{\pi}{2}) J_{2n}(a\xi) & \text{if } \xi \neq 0 \quad n = 0, 1, 2, 3 \ldots, \\ 0 & \text{if } \xi = 0 \quad n = 1, 2, 3 \ldots, \\ \frac{\pi}{2} & \text{if } \xi = 0 \quad n = 0. \end{cases} \tag{5.35}$$

*5.2.3.2 Evaluation of $f_{mx}$ and $g_{nx}$.* Applying equation (5.31) to the definition of $f_{mx}$ and $g_{nx}$ yields

$$\begin{aligned} f_{mx}(\xi) &= \int_{-a}^{a} U_{(2m+1)}(\frac{x}{a}) \sqrt{1-(\frac{x}{a})^2} e^{jx\xi} dx \\ &= \underbrace{\int_{-a}^{a} U_{(2m+1)}(\frac{x}{a}) \sqrt{1-(\frac{x}{a})^2} \cos(x\xi) dx}_{=0} + j \int_{-a}^{a} U_{(2m+1)}(\frac{x}{a}) \sqrt{1-(\frac{x}{a})^2} \sin(x\xi) dx \\ &= 2aj \int_{0}^{1} U_{(2n+1)}(\tilde{x}) \sqrt{1-(\tilde{x})^2} \sin(a\tilde{x}\xi) d\tilde{x} \\ &= 2ajI^{o}_{fmx}(a\xi) \end{aligned} \tag{5.36}$$

and

$$\begin{aligned} g_{mx}(\xi) &= \int_{-a}^{a} U_{(2n+1)}(\frac{x}{a})\sqrt{1-(\frac{x}{a})^2}e^{-jx\xi}dx \\ &= \underbrace{\int_{-a}^{a} U_{(2n+1)}(\frac{x}{a})\sqrt{1-(\frac{x}{a})^2}\cos(x\xi)dx}_{=0} - j\int_{-a}^{a} U_{(2n+1)}(\frac{x}{a})\sqrt{1-(\frac{x}{a})^2}\sin(x\xi)dx \\ &= -2aj\int_{0}^{1} U_{(2n+1)}(\tilde{x})\sqrt{1-(\tilde{x})^2}\sin(a\tilde{x}\xi)d\tilde{x} \\ &= -2ajI^{o}_{gnx}(a\xi) \end{aligned} \tag{5.37}$$

where (see Appendix A)

$$I^{o}_{fmx}(a\xi) = I^{o}_{gnx}(a\xi) = \begin{cases} (-1)^n(\frac{(n+1)\pi}{a\xi})J_{2n+2}(a\xi) & \text{if } \xi \neq 0 \quad n = 0,1,2,3\ldots, \\ 0 & \text{if } \xi = 0. \end{cases} \tag{5.38}$$

*5.2.3.3 Asymptotical Behavior of Integrands.* Again, the behavior of the integrands must be investigated prior to performing numerical integration. Using (5.26) and the large argument approximation of the Bessel function, the behavior of the integrands as $\xi \to \infty$ is given by

$$\lim_{\xi\to\infty} I(A_{xx}) \sim \frac{1}{\xi^2} \tag{5.39}$$

$$\lim_{\xi\to\infty} I(A_{xz}) \sim \frac{1}{\xi^2} \tag{5.40}$$

$$\lim_{\xi\to\infty} I(A_{zx}) \sim \frac{1}{\xi^2} \tag{5.41}$$

$$\lim_{\xi\to\infty} I(A_{zz}) \sim \frac{1}{\xi^2} \tag{5.42}$$

Additionally, when analyzing the behavior for small arguments, only the worst case scenario $(n, m = 0)$ need be considered. The behavior of the integrands as $\xi \to 0$ is

found to be

$$\lim_{\xi\to 0} I(A_{xx}) \sim \xi^2 \tag{5.43}$$

$$\lim_{\xi\to 0} I(A_{xz}) \sim \xi^2 \tag{5.44}$$

$$\lim_{\xi\to 0} I(A_{zx}) \sim \xi^2 \tag{5.45}$$

$$\lim_{\xi\to 0} I(A_{zz}) \sim 0 \tag{5.46}$$

where $I(A^{mn}_{\alpha\beta})$ is the integrand of the integral corresponding to $A^{mn}_{\alpha\beta}$. At both extremes ($\xi \to \infty$ and $\xi \to 0$), the integrands are well behaved and thus suitable for numerical integration. Substantial acceleration of convergence is achieved using these more well-behaved expansion and testing functions. Thus, numerical integration can be used to compute the MoM matrix elements.

*5.2.3.4 Solving the System $\boldsymbol{A}x = 0$.* Based on the second scenario for the testing and expansion functions, the MoM matrix equation for the natural modes is written as

$$\begin{bmatrix} A^{mn}_{xx} & A^{mn}_{xz} \\ A^{mn}_{zx} & A^{mn}_{zz} \end{bmatrix} \begin{bmatrix} a_{xn} \\ a_{zn} \end{bmatrix} = \begin{bmatrix} 0 \\ 0 \end{bmatrix} \tag{5.47}$$

where (using the evenness of integrands)

$$A^{mn}_{xx} = 8a^2 \int_0^\infty (k^2 - \xi^2)\tilde{\tilde{G}}_{xx}(\xi, \zeta, y_o|y_o) I^o_{fxm}(a\xi) I^o_{gxn}(a\xi) d\xi \tag{5.48}$$

$$A^{mn}_{xz} = 8a^2 j \int_0^\infty -\xi\zeta\tilde{\tilde{G}}_{zz}(\xi, \zeta, y_o|y_o) I^o_{fxm}(a\xi) I^e_{gzn}(a\xi) d\xi \tag{5.49}$$

$$A^{mn}_{zx} = -8a^2 j \int_0^\infty -\xi\zeta\tilde{\tilde{G}}_{xx}(\xi, \zeta, y_o|y_o) I^e_{fzm}(a\xi) I^o_{gxn}(a\xi) d\xi \tag{5.50}$$

$$A^{mn}_{zz} = 8a^2 \int_0^\infty (k^2 - \zeta^2)\tilde{\tilde{G}}_{zz}(\xi, \zeta, y_o|y_o) I^e_{fzm}(a\xi) I^e_{gzn}(a\xi) d\xi. \tag{5.51}$$

This matrix equation will have a non-trivial solution only if the determinant is equal to zero [36]. There are an infinite number of $\zeta$ values leading to $det(A) = 0$ and it is these values that represent the propagation constant of the natural modes of

the stripline structure. Once the natural mode propagation constants are found, the natural mode currents (i.e.,$a_{nx}$ and $a_{nz}$) can be easily computed using an eigenvector solution technique. In this research, only the TEM natural mode behavior is sought and discussed next.

*5.2.3.5 Numerical Results.* Except for the evaluation of $g_{n\alpha}$ and $f_{m\alpha}$ $(\alpha = x, z)$ all integrations were performed numerically. Matlab's adaptive Simpson quadrature rule was used exclusively to compute the matrix elements. A second routine, a secant method root search, was used to find the value of $\zeta$ that would make the MoM impedance matrix singular. The null space of the system was found using Matlab; however, numerical errors produced only a "nearly singular" impedance matrix. To ensure the nullspace was not empty, an LU matrix factorization was performed and the value of the $N^{th}$ row and $N^{th}$ column of the resulting reduced matrix was reset to zero. To verify the correct answer was used to compute the current, the eigenvector corresponding to the smallest eigenvalue was also used. This process provided a method to check the accuracy of the integration results. As the precision of integration improved, the magnitude of the smallest eigenvalue converged to zero as expected. The numerical results and effort to optimize the code will be discussed in the following sections.

The algorithms designed to integrate and populate the impedance matrix can be found in Appendix B. It was designed to be accurate and efficient. A special function was used to select the upper limit of integration to ensure sufficient convergence was achieved. As seen in Figure 5.2, the the value for $A_{xx}^{mn}$ is found to the thousands decimal place. At these large values of $\xi$, the oscillating integrand is nearly symmetrical about the $\xi$-axis and the contribution of the integrand beyond the limits displayed in Figure 5.2 can be neglected. Similar convergence is expected for the remaining integrals, since they all converge at the same rate (see equations (5.39)-(5.42)). Efficiency can be improved by exploiting the symmetries of the impedance matrix. The $A_{xx}^{mn}$ and $A_{zz}^{mn}$ quadrants are both diagonally symmetry. Only the diagonal and upper

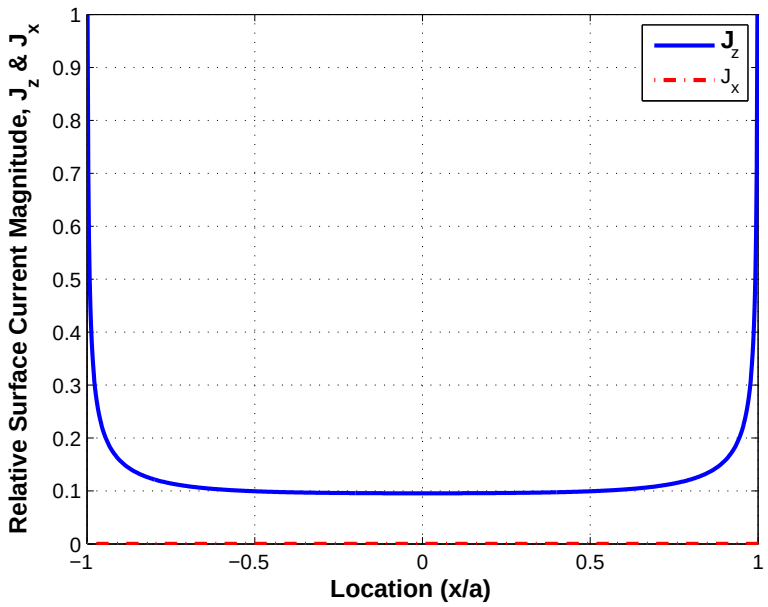


Figure 5.1: Cross Sectional Currents Found on a Perfectly Conducting Center Conductor. These values were found for at a frequency of 10 MHz for a stripline with 3.46 cm ground plane spacing and a center conductor 5 cm wide.

off-diagonal terms need to be calculated. The $A_{zx}^{mn}$ and $A_{xz}^{mn}$ quadrants are complex transposes; thus, only values for one of these quadrants needs to be computed. Exploiting these properties reduces the numbers integrations needed to fill the impedance matrix from $4(N)^4$ to $2(N)^2 + (N)$ and reduces the computational time for filling the matrix by 26 percent. Furthermore, It will be shown in the next chapter that no more than three expansion terms are needed to accurately compute the characteristic impedance, producing a 6x6 impedance matrix.

Using the algorithms included in Appendix B, the $x$ and $z$ components of the current and guided propagation constant were computed. The currents are displayed in Figure 5.1. As anticipated, the TEM mode is being maintained exclusively by the longitudinal component of the current ($J_z$). Furthermore, the distribution of the current on the strip adheres to well established current behavior [17]. The value of the computed wave number ($\zeta = k = \omega\sqrt{\epsilon\mu}$), agrees with physical intuition, namely that a forward propagating $z$-directed wave behaves like $e^{(-j\zeta z)}$, where $\zeta = \beta - j\alpha$. For

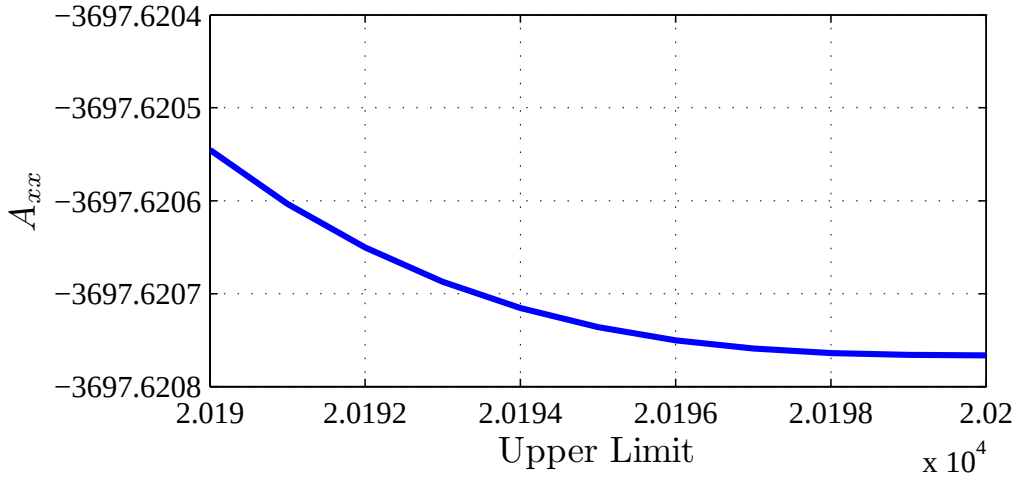


Figure 5.2: Convergence achieved through special algorithm (see Appendix B) that selected the optimal upper limit.

PEC boundaries, there are no losses ($\alpha = 0$) and we have $e^{(-j\beta z)}$, a pure propagating wave with no decay. The computed currents and wave number will be used in the next chapter to calculate the characteristic impedance of the lossless stripline.

### *5.3 MoM Solution of the Integral Equation for Specialized TEM Case*

In Chapter 4, a specialized integral equation was formulated for the TEM mode of the stripline having a PEC center conductor. It was shown that the generalized EFIE formulation reduces to the single integral equation (5.52),

$$\int_{-a}^{a}\int_{-\infty}^{\infty} k\xi\tilde{\tilde{G}}_{zz}(\xi,k;y_0 \mid y_0)e^{j\xi x}e^{-j\xi x'}\tilde{J}_{sz}(x')d\xi dx', \tag{5.52}$$

under the condition that $\zeta = k$ and $\tilde{J}_{sx} = 0$ (which is consistent with the previous section). This integral equation can be solved using the expansion and testing functions of the previous section, namely $e_{nz}(x)$ and $t_{mx}(x)$. Performing the necessary

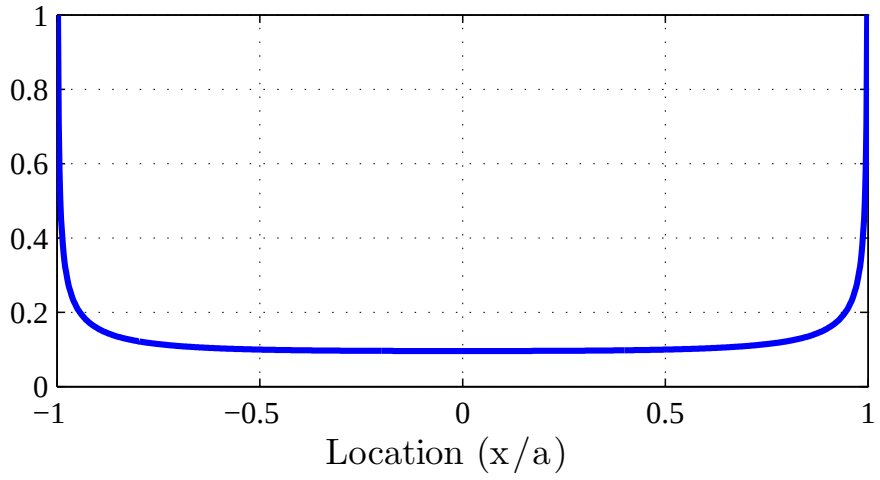


Figure 5.3: Cross Sectional Current, $\tilde{J}_{sz}$, obtained using the TEM specialization IE for N=3, frequncy=10 MHz.

expansion and testing leads to the matrix equation

$$\sum_{n=0}^{N-1} a_{nz} A_{xz}^{mn} = 0 \ldots m = 0, \ldots, N-1 \tag{5.53}$$

where

$$A_{xz}^{mn} = \int_0^\infty \tilde{\tilde{G}}_{zz}(\xi, \zeta, y_0 \mid y_0) J_{2n}(a\xi) J_{2m+2}(a\xi) d\xi. \tag{5.54}$$

Note, as in the previous section, evenness of the integrand reduces the limits of integration from $(-\infty, \infty)$ to $(0, \infty)$ and the leading constants were removed due to the homogeneous nature of the matrix equation.

It is shown in Figure 5.4 that the coupled and specialized equation integral equations for the TEM mode current $\tilde{J}_{sz}$ produce identical results as anticipated. However, it is noted that the resulting specialized integral equation MoM matrix contains $N^2$ elements as opposed to $4N^2$ elements in the coupled IE formulation. This results a tenfold improvement in computational efficiency.

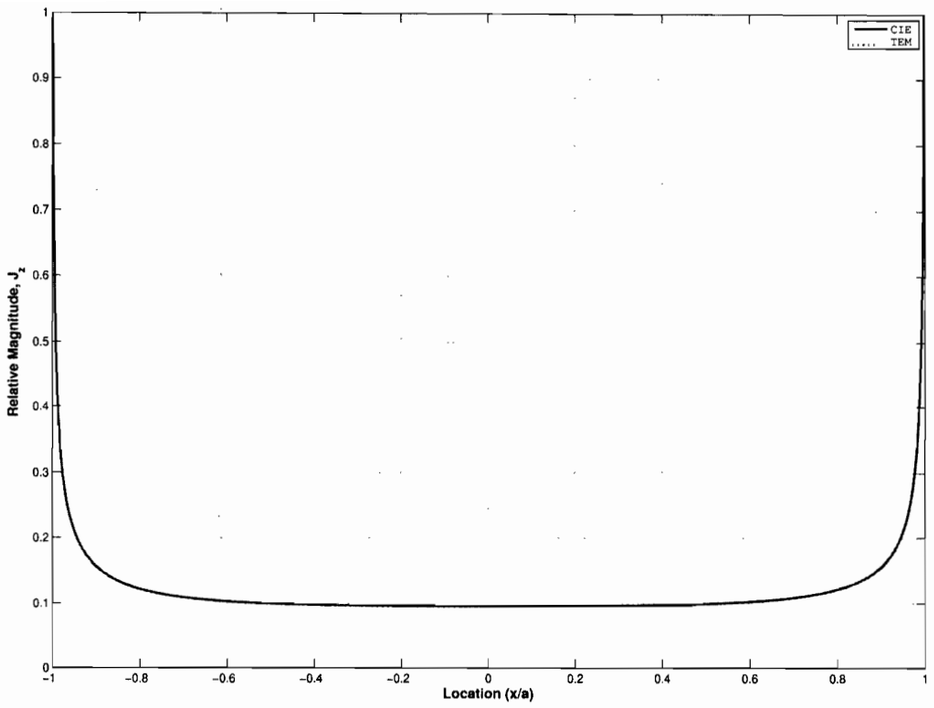


Figure 5.4: Comparison of both MoM solutions.

## *5.4 Summary*

In this chapter, a MoM solution was sought for the IEs formulated in Chapter 4. For the CIE formulated for the stripline with a PEC center conductor, a Galerkin's based MoM solution using Chebsyshev polynomials of the first and second kind yielded the unknown currents and propagation constant. This approach was also used to find a very computationally efficient solution to the specialized TEM integral equation. In the next chapter, the currents found will used to calculate the characteristic impedance of the stripline.

# VI. Characteristic Impedance

The culmination of the design process is to ensure that the specified stripline design parameters will produce the required characteristic impedance. In Chapter 2, the ground plane spacing was calculated to provide the necessary operational frequency regime. In addition, an approximate value for the center conductor width was computed. In this chapter, an expression to compute the characteristic impedance of the stripline will be developed using the MoM solution obtained in Chapter 5. This expression will be used to test the accuracy of the proposed center conductor width. Any essential modifications to the design will be identified. Furthermore, the physical understanding of stripline characteristic impedance will be supplemented by viewing the stripline as a pair of parallel capacitors. Using this simplified model will provide an indication of factors impacting the characteristic impedance of a stripline. Finally, the effects of center conductor misalignment on characteristic impedance will be investigated.

## *6.1 Derivation of Full Wave Expression for the Characteristic Impedance of a Stripline*

In this section, an expression for the characteristic impedance will be developed using the MoM solution obtained in Chapter 5. An expression for the characteristic impedance (for a forward traveling wave) of a stripline with PEC ground planes and an infinitesimally thin PEC center conductor will be calculated using the relation

$$Z_o = \frac{V}{I}, \tag{6.1}$$

where

$$V = -\int_C \vec{E} \cdot \vec{dl} \ldots C \text{ extends from the center conductor to the ground plane} \tag{6.2}$$

and

$$I = \oint_{cs} \vec{J} \cdot \hat{n} dS. \tag{6.3}$$

By exploiting the infinite range of the stripline along the guiding axis, $z$ (transforming to the $\zeta$-domain), using a current of the form $\vec{J} = \hat{z} J_{sz}(x)\delta(y - y_o)$ and selecting the most advantageous path of integration ($\vec{dl} = \hat{y}dy$, $\hat{n} = \hat{z}$ and $dS = dxdy$), equations (6.3) and (6.2) can be greatly simplified. The remainder of this section will outline the derivation of the expression used to compute the characteristic impedance.

The spectral version of the characteristic impedance is given by

$$\tilde{Z}_o = \frac{\tilde{V}}{\tilde{I}} \tag{6.4}$$

where

$$\tilde{V} = -\int_C \tilde{\vec{E}} \cdot \vec{dl} \ldots C \text{ extends from the center conductor to the ground plane} \tag{6.5}$$

and

$$\tilde{I} = \oint_{cs} \tilde{\vec{J}} \cdot \hat{n} dS. \tag{6.6}$$

Substituting $\vec{dl} = \hat{y}dy$ in the expression (6.5) yields

$$\tilde{V} = -\int_h^{y_0} \tilde{E}_y^s dy \tag{6.7}$$

where

$$\tilde{E}_y^s = \frac{\partial}{\partial y} \frac{\zeta_n}{\omega \epsilon \mu} \tilde{A}_z^s(0, y, \zeta_n). \tag{6.8}$$

Using Leibniz's rule [8], the voltage can be found by evaluating $\tilde{A}_z(0, y, \zeta_n)$ at the limits of integration. Recalling that $\tilde{A}^s_z(x, y, \zeta_n)$ is given by

$$\begin{aligned}\tilde{A}^s_z(x, y, \zeta_n) &= \int_{-a}^{a} \tilde{G}_{zz}(x, \zeta; y_0 \mid y_0)\mu\tilde{J}^s_{zs}(x')dx' \\ &= \int_{-a}^{a} \frac{1}{2\pi}\int_{-\infty}^{\infty} \tilde{\tilde{G}}_{zz}(\xi, \zeta; y_0 \mid y_0)e^{jx\xi}e^{-jx'\xi}\mu\tilde{J}^s_{zs}(x')d\xi dx'. \end{aligned} \tag{6.9}$$

As expected, $\tilde{A}^s_z(0, h, \zeta_n)$ (the upper boundary) is identically zero. The voltage is merely $-\frac{\zeta}{j\omega\epsilon\mu}\tilde{A}^s_z(0, y_o, \zeta_n)$.

The calculation of $\tilde{A}^s_z(0, y_o, \zeta_n)$ is very straight forward when the results of the previous chapter are used. Using the expansion of the current defined in Chapter 5, the voltage is given by

$$\tilde{V} = \frac{\zeta}{j\omega\epsilon\mu}\tilde{A}_z(0, y_o, \zeta_n) = \frac{a\zeta_n}{\pi\omega\epsilon}\sum_{n=0}^{N-1} a_{nz}\int_{-\infty}^{\infty} \tilde{\tilde{G}}_{zz}(\xi, \zeta_n; y_0 \mid y_0)I^e_{gnz}(\xi)d\xi \tag{6.10}$$

Additionally, the current reduces to

$$\tilde{I} = a\pi a_{z0} \tag{6.11}$$

where $a$ is the half-width of the center conductor and $a_{z0}$ is the leading expansion coefficient for the longitudinal current $\tilde{J}_{sz}$ [17].

Substituting the newly found expression for the spectral voltage and current into (6.4) leads to the follow expression for the characteristic impedance of the lossless stripline operating in the TEM mode;

$$\tilde{Z}_o = \frac{\sqrt{\mu}}{\pi^2\sqrt{\epsilon}}\sum_{n=0}^{N-1}\frac{a_{nz}}{a_{0z}}\int_0^{\infty}\frac{\cosh 2ph - \cosh 2py_o}{2p\sinh 2ph}I^e_{gnz}(\xi)(\xi)d\xi. \tag{6.12}$$

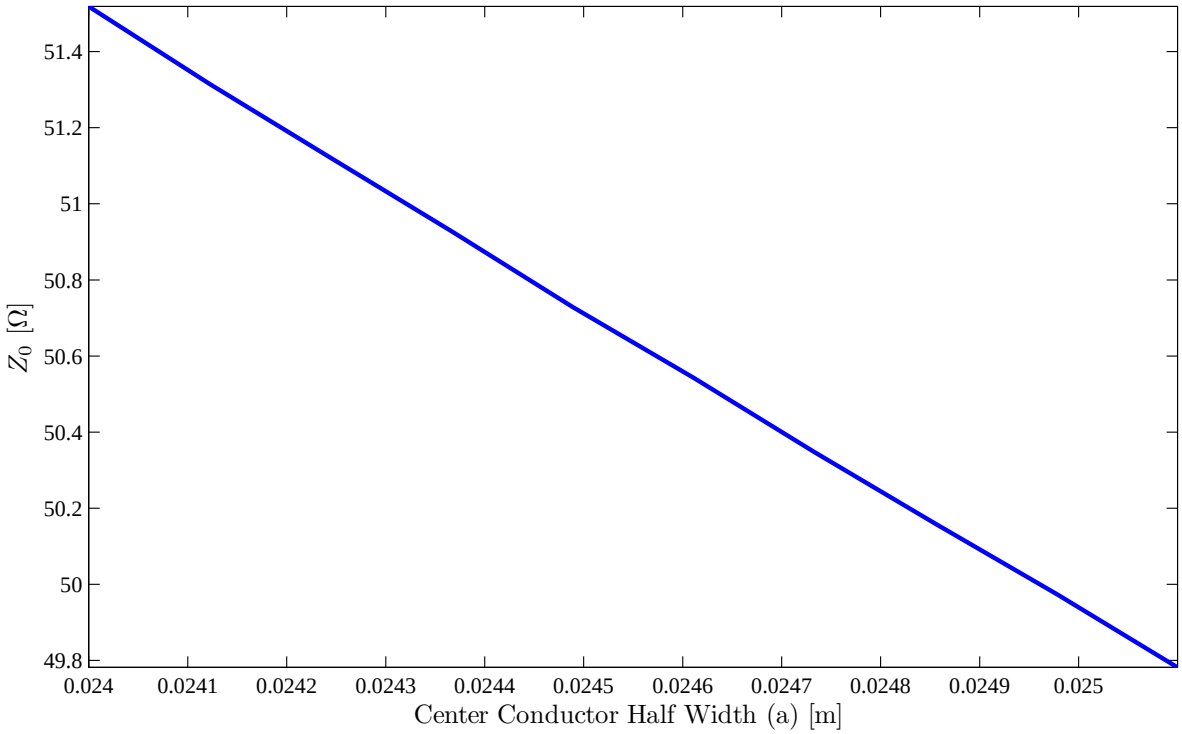


Figure 6.1: The Effects of Center Conductor Width on Characteristic Impedance.

This expression will be used to determine the width of the stripline field applicator's center conductor and to investigate the effects of center conductor misalignment.

### *6.2 Validation of AFRL's Design*

Expression (6.12) was evaluated with the approximate physical parameters supplied by AFRL. Letting $h = .0173$ and $a = .025$, yielded a characteristic impedance of 49.76 ohms.

While this is close to the desired value, 50 ohms, some adjustments are warranted. A thinner center conductor will provide a characteristic impedance closer to the desired value, as seen in Figure 6.1. Re-evaluating expression (6.12) with center conductor width of 2.496 cm leads to a characteristic impedance of 50.09 ohms. Note, more precise characteristic impedance can be computed if supported by fabrication

methods. These results, as will be demonstrated in the next section, correspond with physical intuition.

*6.2.1 Physical Interpretation.* To ensure reasonable results were obtained in the previous section, it is useful to investigate the physical phenomenon of characteristic impedance. In this section, a common approximation for the characteristic impedance will be used [5, 31]. This approximation will provide excellent results for TEM mode propagation and give insight into parameters effecting the characteristic impedance of the stripline [1, 34].

Consider the characteristic impedance of the stripline given by

$$Z_0 = \sqrt{\frac{L}{C}} \tag{6.13}$$

where L is the inductance per unit length and C is the capacitance per unit length [5]. Substituting the phase velocity, given by

$$v_p = \frac{1}{\sqrt{LC}} \tag{6.14}$$

into the expression (6.13) leads to

$$Z_0 = \frac{1}{v_p C} = \frac{\sqrt{\mu\epsilon}}{C} \tag{6.15}$$

where C is the total capacitance of the stripline. Neglecting fringe capacitance, a stripline can be considered as two capacitors in parallel, $C = C_u + C_l$, where the total capacitance is the sum of the capacitance between the center strip and the upper ground plane ($C_u$) and the capacitance between the center conductor and the lower ground plane ($C_l$). The upper and lower capacitances can be calculated according to the expression given by

$$C_\beta = \frac{\epsilon A}{d_\beta} \quad \beta = u, l \tag{6.16}$$

where $d_\beta$ is the distance between the the center conductor and the corresponding ground plane, A is the area of the plates and $\epsilon$ is the permittivity of the material between the center conductor and the ground planes. It is clear that variations in the spacing of the ground planes ($h$) and the width of the center conductor ($a$) will influence the characteristic impedance. Increasing the width of the center conductor increases the area of the capacitors and will decrease the characteristic impedance, as seen in Figure 6.1. Increasing the spacing between the ground planes increases the distance between the plates of the capacitors and the characteristic impedance increases. Insight gained in this section can also provide insight into the effects of center conductor misalignment.

### *6.3 Effects of Center Conductor Misalignment*

Building on insight gained in the previous section, the effects of center conductor misalignment will be investigated. First, the capacitor model will be adjusted to accommodate center conductor misalignment. The physical insight gained through this process will be used to verify results obtained by computing the characteristic impedance of the stripline applicator with various levels of center conductor misalignment. Finally, further verification will be accomplished through CEM simulation.

To accommodate center conductor misalignment, the total capacitance of the stripline can be written as

$$\begin{aligned} C &= C_u + C_l \\ &= \frac{\epsilon A}{h - y_0} + \frac{\epsilon A}{h + y_0} \\ &= \epsilon A(\frac{1}{h - y_0} + \frac{1}{h + y_0}) \\ &= \frac{\epsilon A}{h}(\frac{1}{1 - y_0/h} + \frac{1}{1 + y_0/h}). \end{aligned} \tag{6.17}$$

When the stripline is perfectly aligned ($y_0 = 0$) the total capacitance is given by

$$C = \frac{2\epsilon A}{h}. \tag{6.18}$$

Similarly, for small degrees of misalignment ($y_0 << 1$) equation(6.19) can be rewritten as

$$\begin{aligned} C &= \frac{2\epsilon A}{h}(\frac{1}{1-(y_0/h)^2}) \\ &= \frac{2\epsilon A}{h}(1-(\frac{y_0}{h})^2 + \ldots), \end{aligned} \tag{6.19}$$

which reduces to

$$C = \frac{2\epsilon A}{h}. \tag{6.20}$$

Thus, small degrees of center conductor misalignment ($y_0 \sim 0$) will not strongly impact the characteristic impedance. Additionally, as the displacement of the center conductor increases the total capacitance increases and consequently the characteristic impedance is driven down. This will be demonstrated in the following section as the characteristic impedance of the stripline is computed at various levels of center conductor displacement.

The characteristic impedance was computed using expression (6.12) evaluated at various values of center conductor displacement. When perfectly alignment ($y_0 = 0$), the characteristic impedance is nearly 50 ohms. As predicted above, the characteristic impedance of the stripline decreases as the center conductor migrates to the upper ground plane (see Figures 6.2). However, the characteristic drops more rapidly than expected, as seen in Figure 6.2. Examination of the electric field for the stripline with the center conductor located at $y_o = .5h$ (see Figure 6.3) reveals that the electric field lines fringe from the bottom of the center conductor to the upper ground plane, effectively increasing the area of the fringe capacitors. Thus, the parallel capacitor model is limited in its ability to predict the effects of center conductor misalignment. Due to the discrepancies between the expected and computed values of characteristic

impedance, additional verification of the effects of center conductor misalignment was obtained through Microwave Studio simulation (see Figure 6.4) [35]. The simulated and computed results agreed (see Figure 6.2). Thus with confidence, expression (6.12) predicts the effects of center conductor misalignment.

Expression (6.12) was also evaluated using various numbers of expansion terms. As seen in Figure 6.5, it is accurate when as few as three expansion terms are used. The results for the characteristic impedance using more than three expansion terms are identical. While using two expansion terms provides a close solution, greater accuracy can be gained by adding more terms. Using a single expansion term ($N = 1$) or trying to model the current with a zeroth order Chebsyshev polynomial (constants for both the first and second kind of Chebsyshev polynomials) results in a poor solution.

## *6.4 conclusion*

In this chapter, a full wave expression was developed to calculate the characteristic impedance of a stripline using the MoM solution obtained in the previous chapter. It was used to recommend that the width of the center conductor for AFRL's stripline field applicator be reduced to 4.992 cm. The change will bring the characteristic impedance closer to the desired 50 ohms. Additionally, the effects on the characteristic impedance due to center conductor misalignment were examined. As the center conductor approaches the ground plane the characteristic impedance drops. However, small variation in center conductor alignment do not strongly influence the characteristic impedance.

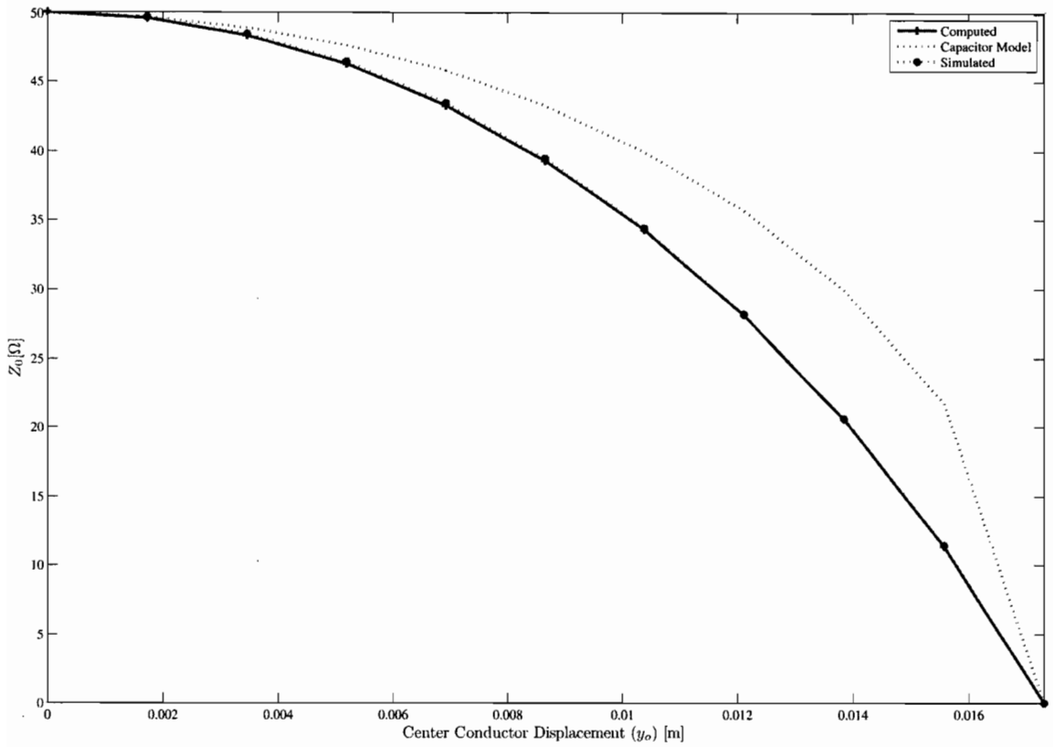


Figure 6.2: The Effects of Center Conductor Misalignment on Characteristic Impedance.

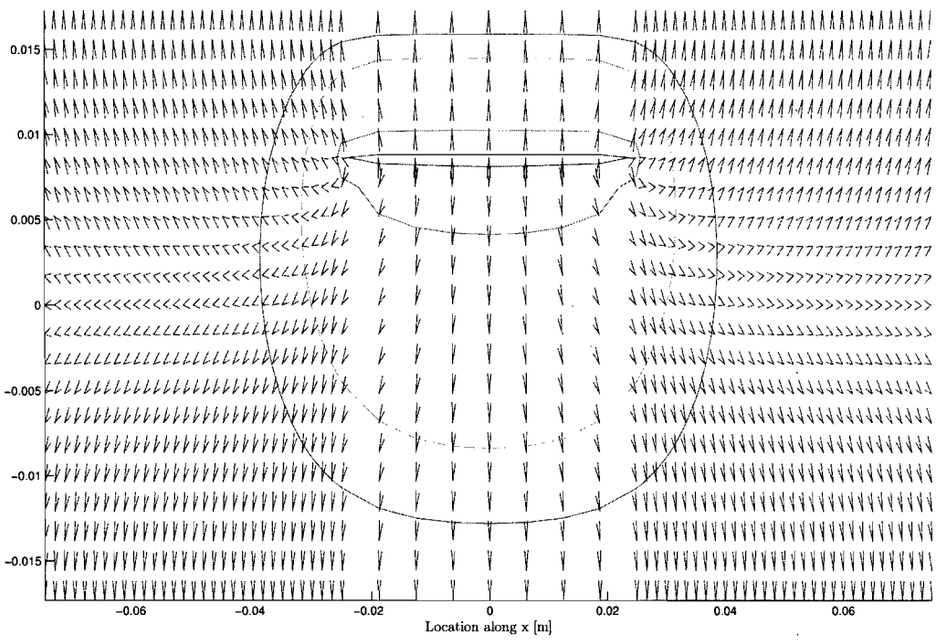


Figure 6.3: Effects of Center Conductor Misalignment of Electric Field.

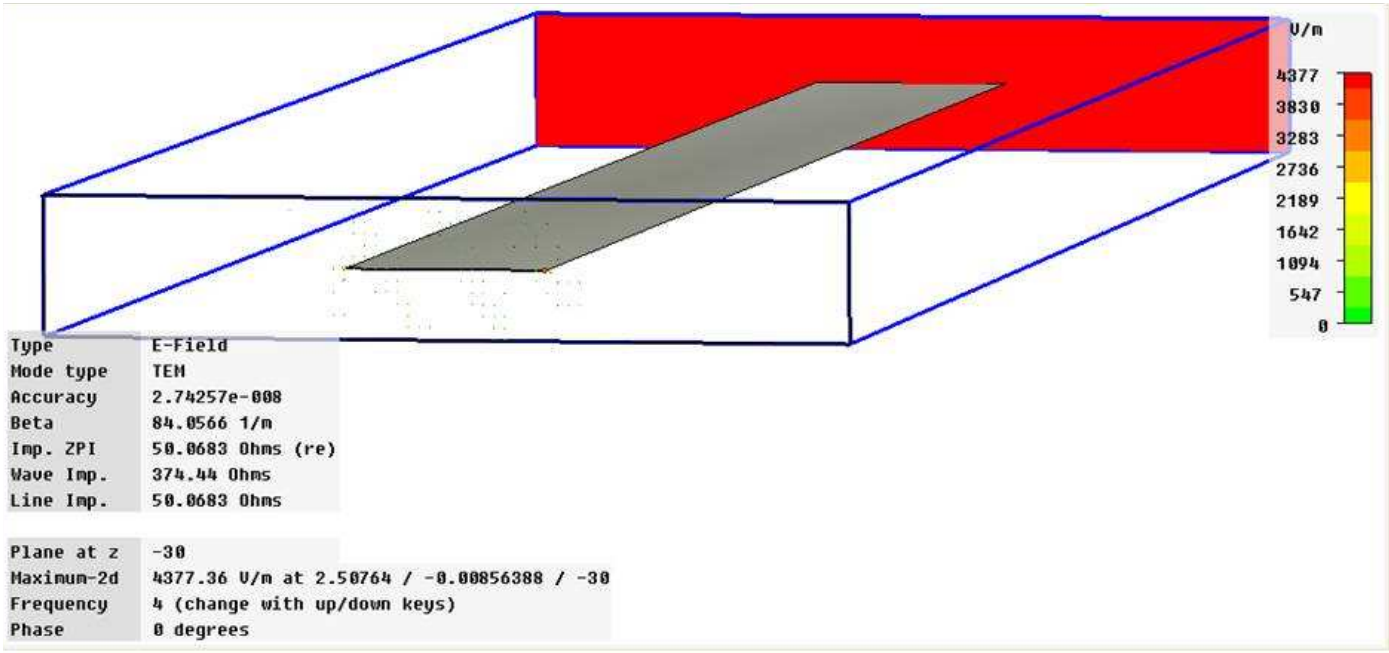


Figure 6.4: Microwave Studio CAD Model and Simulation Results.

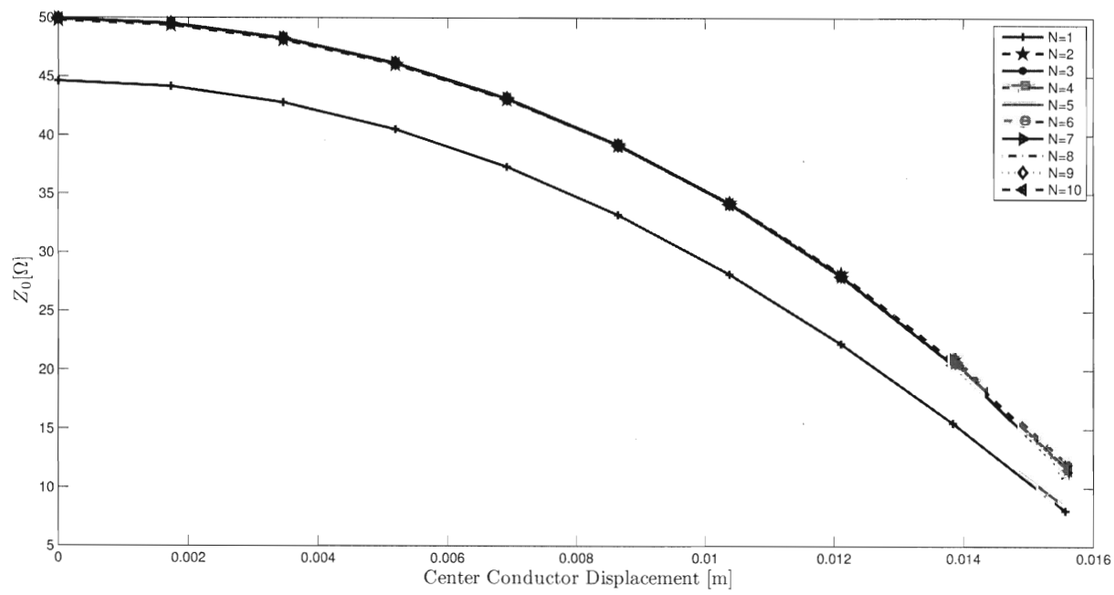


Figure 6.5: The Effects of Number of Expansion Terms (N) on Characteristic Impedance.

# VII. Conclusion

In conclusion, this research reviewed the approximate design parameters proposed for the design of a stripline that will be used to test the electromagnetic properties of materials at high temperature and low frequency. It began by summarizing fundamental concepts from transmission theory. The properties of stripline were examined. Additionally, the stripline design process and a few stripline applications were presented. It also briefly reviewed recent developments in stripline fabrication. Next, the vector potential parallel-plate Green's function for an electric current was developed using the spectral and spacial vector potential boundary conditions for the parallel-plate wave guide. The subsequent forced vector potential wave equation was solved by decomposing the equation into principle and reflective parts. Each part was then solved independently. Complex analysis was used to find the solution to the principle part and the reflected part was readily identified as having a harmonic solution. Boundary conditions were applied to the total solution at the outer conductors to find the Green's function. Next, a compact hyperbolic version of the Green's function was identified and used to formulate an integral equation for a stripline. A pair of coupled integral equations were formulated for a stripline having a perfect center conductor. Furthermore, it was shown that the coupled integral equation reduce to a single integral equation for the TEM mode. This specialization naturally led to a more computationally efficient formulation. Next, the solution of these integral equations was obtained employing a Galerkin's-based MoM solution using Chebsyshev polynomials as expansion and testing functions. The unknown center conductor currents and guiding axis propagation constant were then used to formulate an expression for the characteristic impedance. The expression was used to analyze the approximate design parameters of AFRL's stripline field applicator and examine the effects of center conductor misalignment. It was used to recommend that the center conductor for AFRL's stripline field applicator be reduced to 4.992 cm. The change will bring the characteristic impedance closer to the desired 50 ohms. Additionally, as the center conductor approaches the ground plane the characteristic impedance drops.

However, small variation in center conductor alignment do not strongly influence the characteristic impedance.

## *7.1 Contributions*

This design verification and characteristic impedance understanding will pave the way in giving Air Force Research Laboratory the capability of measuring shielding materials at low frequencies and high temperatures.

## *7.2 Future Research*

During this research, much was learned about the behavior of striplines. In spite of this, much work in this area remains. Adding thickness to the center conductor, extending the research to striplines that are variant along the guiding axis, replacing PEC with lossy high temperature alloys and finding an analytical solution for the integrals encountered while obtaining the method of moments solution would be very interesting.

Literature indicates that replacing the infinitesimally thin center conductor with an actual center conductor with finite thickness will improve characteristic impedance calculation accuracy [10].

This research was limited to uniform center conductor misalignment. Utilizing non-uniform transmission line theory where the capacitance is dependent on position may yield insight into non-uniform center conductor alignment.

Facilitating high temperature material characterization measurements necessitates use of high temperature alloys in stripline construction. The conductivity of high temperatures alloys is significantly lower than the conductivity of traditional room temperature conductors, as seen in Table 7.1. The effects of a lossy center conductor on the characteristic impedance and propagating characteristics of the stripline should be investigated to improve the accuracy of high temperature material characterization measurements.

Table 7.1: The conductivity of high temperatures alloys is significantly lower than the conductivity of traditional conductors.

| Metal | Conductivity |
|---|---|
| Copper | $5.9 \times 10^7$ |
| H-214*( at 2200 deg F) | $8.1 \times 10^5$ |
| H-230*(at 1800 deg F) | $7.9 \times 10^5$ |
| HR-120*(at 2200 deg F) | $7.7 \times 10^5$ |
| H-282*(at 1800 deg F) | $7.6 \times 10^5$ |
| * High temperature alloys produced by Haynes International, Inc. | |

There has also been success in finding analytical solutions to integral equations resulting from similar geometries. [12,13,38] An analytical solution using a pole series expansion or special function could dramatically increase computational efficiency.

# *Appendix A. Chebsyshev Polynomials*

This appendix lists the expressions and formulas used in evaluating integrals containing Chebsyshev polynomials encountered in the MoM solution of Integral Equations. The main reference is [7, 17, 33].

Throughout the appendix, $T_n(x)$ will specify a Chebsyshev polynomials of the first kind of order $n$. Likewise, $U_n(x)$ will indicate a Chebsyshev polynomials of the second kind of order $n$.

Chebsyshev polynomials of the first kind were generated using the following recursive relations, given as

$$T_n(x) = 2xT_{n-1}(x) - T_{n-2}(x) \tag{A.1}$$

A few Chevbsyshev polynomials of the first kind can be given as

$$\begin{aligned} T_0(x) =& 1 \\ T_1(x) =& x \\ T_2(x) =& 2x^2 - 1 \\ T_3(x) =& 4x^3 - 3x \\ T_4(x) =& 8x^4 - 8x^2 + 1 \\ T_5(x) =& 16x^5 - 20x^3 + 5x \end{aligned} \tag{A.2}$$

(A.3)

Chebsyshev polynomials of the second kind were generated using the following recursive relations, given as

$$U_n(x) = 2xU_{n-1}(x) - U_{n-2}(x) \tag{A.4}$$

A few Chevbsyshev polynomials of the second kind can be given as

$$\begin{aligned} U_0(x) =& 1 \\ U_1(x) =& 2x \\ U_2(x) =& 4x^2 - 1 \\ U_3(x) =& 8x^3 - 4x \\ U_4(x) =& 16x^4 - 12x^2 + 1 \\ U_5(x) =& 32x^5 - 32x^3 + 6x \end{aligned} \tag{A.5}$$

(A.6)

### *A.1 Preliminary Expressions*

The follow expressions are used to evaluate the integrals involving Chebsyshev Polynomials encountered in Chapter 5

$$T_n(-x) = (-1)^n T_n(x) \tag{A.7}$$

$$e^{jx} = \cos x + j \sin x \tag{A.8}$$

$$T_n(\cos\theta) = \cos n\theta \tag{A.9}$$

$$\sin^2\theta = 1 - \cos^2\theta \tag{A.10}$$

$$\sin^2\theta = \frac{1 - \cos 2\theta}{2} \tag{A.11}$$

$$\cos A \cos B = \frac{1}{2}[\cos(A+B) + \cos(A-B)] \tag{A.12}$$

$$\sin x = \frac{e^{jx} - e^{-jx}}{2j} \tag{A.13}$$

$$\frac{\pi}{(-j)^n} J_n(x) = \int_0^\pi \cos n\theta e^{jx\cos\theta} d\theta \tag{A.14}$$

$$J_n(\tilde{a}e^{jm\pi}) = e^{jmn\pi} J_n(\tilde{a}) \ldots m = integer \tag{A.15}$$

### *A.2 Integrals with Chebsyshev Polynomials*

Some of the integrals involving Chebsyshev Polynomials encountered in MoM solutions. Proofs to these integrals are available in literature [7, 17, 33].

$$\int_0^1 \frac{T_n(x)}{\sqrt{1-x^2}} \cos \tilde{a}x dx = \begin{cases} (-1)^{n/2}(\pi/2)J_n(\tilde{a}) & \text{if } \tilde{a} \neq 0 \text{ and } n = 0, 2, 4 \dots \\ \frac{\pi}{2} & \text{if } \tilde{a} = 0 \text{ and } n = 0 \\ 0 & \text{if } \tilde{a} = 0 \text{ and } n = 2, 4 \dots \end{cases} \tag{A.16}$$

$$\int_0^1 U_n(x)\sqrt{1-x^2} \sin \tilde{a}x dx = \begin{cases} (-1)^{(n-1)/2} \frac{(n+1)\pi}{\tilde{a}}(\pi/2)J_{n+1}(\tilde{a}) & \text{if } \tilde{a} \neq 0 \text{ and } n = 1, 3, 5 \dots \\ 0 & \text{if } \tilde{a} = 0 \text{ and } n = 1, 3, 5 \dots \end{cases} \tag{A.17}$$

### *A.3 Asymptotic Form of Integrals Involving $T_n(x)$ and $U_n(x)$*

The above integrals have the following asymptotic behavior

$$\lim_{\tilde{a}\to\infty} \int_0^1 \frac{T_n(x)}{\sqrt{1-x^2}} \cos(\tilde{a}x) dx \sim \frac{\cos[\tilde{a} - \frac{\pi}{2}(n + \frac{1}{2})]}{\tilde{a}^{1/2}} \dots n = 0, 2, 4 \dots \tag{A.18}$$

$$\lim_{\tilde{a}\to\infty} \int_0^1 U_n(x)\sqrt{1-x^2} \sin \tilde{a}x dx \sim \frac{\cos[\tilde{a} - \frac{\pi}{2}(n + \frac{3}{2})]}{\tilde{a}^{3/2}} \dots n = 1, 3, 5 \dots \tag{A.19}$$

### *A.4 Evaluation of Integrals Encountered in Chapter 5*

The following integrals were encountered will trying to find a MoM solution to CIE formulated in Chapter 4. These integrals involve the Galerkin based MoM solution using Chebsyshev polynomials of the first kind as expansion functions.

### *A.4.1 Evaluating $f_{mx}(\xi)$ and $g_{nx}(\xi)$ of The First Expansion/Test Function Set.*

$$f_{mx}(\xi) = \int_{-a}^{a} T_{2m+1}(\frac{x}{a})\sqrt{1-(\frac{x}{a})^2}e^{jx\xi}dx \tag{A.20}$$

expanding the exponential using (A.8) yields

$$f_{mx}(\xi) = \int_{-a}^{a} T_{2m+1}(\frac{x}{a})\sqrt{1-(\frac{x}{a})^2}\cos x\xi dx + j\int_{-a}^{a} T_{2m+1}(\frac{x}{a})\sqrt{1-(\frac{x}{a})^2}\sin x\xi dx \tag{A.21}$$

The first term on the right hand side of the expression above vanishes because the integrand is odd leading to

$$f_{mx}(\xi) = j\int_{-a}^{a} T_{2m+1}(\frac{x}{a})\sqrt{1-(\frac{x}{a})^2}\sin x\xi dx \tag{A.22}$$

performing a change of variable, where $\tilde{x} = \frac{x}{a}$ leads to

$$f_{mx}(\xi) = aj\int_{-1}^{1} T_{2m+1}(\tilde{x})\sqrt{1-(\tilde{x})^2}\sin a\tilde{x}\xi d\tilde{x} \tag{A.23}$$

performing a second change of variable where $\tilde{x} = \cos\theta$ yields

$$f_{mx}(\xi) = -aj\int_{\pi}^{0} T_{2m+1}(\cos\theta)\sqrt{1-(\cos\theta)^2}\sin\theta\sin(a\cos\theta\xi)d\theta \tag{A.24}$$

which can be rewritten as

$$f_{mx}(\xi) = aj\int_{0}^{\pi} T_{2m+1}(\cos\theta)\sqrt{1-(\cos\theta)^2}\sin\theta\sin(a\cos\theta\xi)\theta \tag{A.25}$$

substituting (A.16) into the equation above and using (A.10) leads to

$$f_{mx}(\xi) = aj\int_{0}^{\pi} \cos[(2m+1)\theta]\sin^2\theta\sin(a\cos\theta\xi)d\theta \tag{A.26}$$

expanding the $\sin^2\theta$ according to (A.11) leads to

$$f_{mx}(\xi) = \frac{aj}{2}\int_0^{\pi} \cos[(2m+1)\theta](1-\cos 2\theta)\sin(a\cos\theta\xi)d\theta \tag{A.27}$$

which can be rewritten as

$$\begin{aligned} f_{mx}(\xi) &= \frac{aj}{2}\int_0^{\pi} \cos[(2m+1)\theta]\sin(a\cos\theta\xi)d\theta \\ &\quad -\frac{aj}{2}\int_0^{\pi} \cos[(2m+1)\theta]\cos 2\theta\sin(a\cos\theta\xi)d\theta \end{aligned} \tag{A.28}$$

using the identity (A.12) will yield

$$\begin{aligned} f_{mx}(\xi) &= \frac{aj}{2}\int_0^{\pi} \cos[(2m+1)\theta]\sin(a\cos\theta\xi)d\theta \\ &\quad -\frac{aj}{4}\int_0^{\pi} \cos[(2m+3)\theta]\sin(a\cos\theta\xi)d\theta \\ &\quad -\frac{aj}{4}\int_0^{\pi} \cos[(2m-1)\theta]\sin(a\cos\theta\xi)d\theta \end{aligned} \tag{A.29}$$

expanding the sin function according to the definition (A.13) leads to

$$\begin{aligned} f_{mx}(\xi) &= \frac{a}{4}\int_0^{\pi} \cos[(2m+1)\theta]e^{j(a\cos\theta\xi)}d\theta \\ &\quad -\frac{a}{4}\int_0^{\pi} \cos[(2m+1)\theta]e^{-j(a\cos\theta\xi)}d\theta \\ &\quad -\frac{a}{8}\int_0^{\pi} \cos[(2m+3)\theta]e^{j(a\cos\theta\xi)}d\theta \\ &\quad +\frac{a}{8}\int_0^{\pi} \cos[(2m+3)\theta]e^{-j(a\cos\theta\xi)}d\theta \\ &\quad -\frac{a}{8}\int_0^{\pi} \cos[(2m-1)\theta]e^{j(a\cos\theta\xi)}d\theta \\ &\quad +\frac{a}{8}\int_0^{\pi} \cos[(2m-1)\theta]e^{-j(a\cos\theta\xi)}d\theta \end{aligned} \tag{A.30}$$

using (A.14) leads to

$$\begin{aligned} f_{mx}(\xi) &= \frac{a\pi}{4(-j)^{2m+1}} J_{2m+1}(a\xi) \\ &\quad -\frac{a\pi}{4(-j)^{2m+1}} J_{2m+1}(-a\xi) \\ &\quad -\frac{a\pi}{8(-j)^{2m+3}} J_{2m+3}(a\xi) \\ &\quad +\frac{a\pi}{8(-j)^{2m+3}} J_{2m+3}(-a\xi) \\ &\quad -\frac{a\pi}{8(-j)^{2m-1}} J_{2m-1}(a\xi) \\ &\quad +\frac{a\pi}{8(-j)^{2m-1}} J_{2m-1}(-a\xi)dx \end{aligned} \tag{A.31}$$

which, using (A.15) can be rewritten as

$$f_{mx}(\xi) = \frac{ja\pi}{2(-j)^{2m}}[J_{2m+1}(a\xi) + \frac{1}{2}(J_{2m+3}(a\xi) + J_{2m-1}(a\xi))] \tag{A.32}$$

a similar process processes yields the following results for $g_{nx}(\xi)$ where

$$g_{nx}(\xi) = \frac{-ja\pi}{2(-j)^{2n}}[J_{2n+1}(a\xi) + \frac{1}{2}(J_{2n+3}(a\xi) + J_{2n-1}(a\xi))] \tag{A.33}$$

### *A.4.2 Evaluating $f_{mz}(\xi)$ and $g_{nz}(\xi)$ of The First Expansion/Test Function Set.*

$$f_{mz}(\xi) = \int_{-a}^{a} \frac{T_{2m}(\frac{x}{a})}{\sqrt{1-(\frac{x}{a})^2}} e^{jx\xi} dx \tag{A.34}$$

expanding the exponential using (A.8) yields

$$f_{mz}(\xi) = \int_{-a}^{a} \frac{T_{2m}(\frac{x}{a})}{\sqrt{1-(\frac{x}{a})^2}} \cos x\xi dx + j\int_{-a}^{a} \frac{T_{2m}(\frac{x}{a})}{\sqrt{1-(\frac{x}{a})^2}} \sin x\xi dx \tag{A.35}$$

The second term on the right hand side of the expression above vanishes because the integrand is odd leading to

$$f_{mz}(\xi) = \int_{-a}^{a} \frac{T_{2m}(\frac{x}{a})}{\sqrt{1-(\frac{x}{a})^2}} \cos x\xi dx \tag{A.36}$$

performing a change of variable, where $\tilde{x} = \frac{x}{a}$ leads to

$$f_{mz}(\xi) = aj \int_{-1}^{1} \frac{T_{2m}(\frac{x}{a})}{\sqrt{1-(\frac{x}{a})^2}} \cos a\tilde{x}\xi dx \tag{A.37}$$

using (A.16) leads to

$$f_{mz}(\xi) = \begin{cases} (-1)^m(\pi/2)J_{2m}(a\xi) & \text{if } a, \xi \neq 0 \text{ and } m = 0, 1, 2 \dots \\ \frac{\pi}{2} & \text{if } a, \xi = 0 \text{ and } m = 0 \\ 0 & \text{if } a, \xi = 0 \text{ and } m = 1, 2 \dots \end{cases} \tag{A.38}$$

a similar process processes yields Identical following results for $g_{nz}(\xi)$.

The following relations were used to analyze the behavior of the integrands as $\xi \to \infty$ and as $\xi \to 0$

$$\lim_{\tilde{a}\to\infty} J_n(\tilde{a}) = \sqrt{\frac{2}{\pi\tilde{a}}} cos(\tilde{a} - (n + \frac{1}{2})\frac{\pi}{2}) \tag{A.39}$$

$$\lim_{\tilde{a}\to\infty} \int_0^1 \frac{T_n(x)}{\sqrt{1-x^2}} \cos(\tilde{a}x)dx \sim \frac{\cos[\tilde{a} - (n + \frac{1}{2})\frac{\pi}{2}]}{\tilde{a}^{1/2}} \tag{A.40}$$

# *Appendix B. Matlab Code*

This appendix contains all the code used to seek a method of moments solution as described in Chapter5. It is based on code developed by Captain Milo Hyde.

Listing B.1: Method of Moment Solution for Coupled Integral Equation. (appendix3/PropagationConstantSearchChebyCheby12.m)

```
function [prop_const, iter, impedMat, error,Jx,...
    Jz] = PropagationConstantSearchChebyCheby12(freq, h,...
    y_o,tol, W, n, maxIter)
% Based on code developed by Cpt Milo Hyde

% PropagationConstantSearchChebyCheby uses a secant search
% to find the propagation constant of a stripline(Fig-1).  The
% algorithm expands and tests the currents on the stripline's
% center conductor using weighted Chebyshev polynomials of the
% 1st kind.  The initial guess of the algorithm is the free
% space wavenumber, k0.  The algorithm also returns the number
% of iterations it took to reach a solution, the impedance
% matrix, the error, the currents on the stripline's center
% conductor, Jx and Jz, and the characteristic
% impedance, Zc, assuming quasi-TEM, Jx = 0.
%
% Fig-1
%
% ////////////////////PEC//////////////////////////////
% ------------------------------------------------------  y = h
%  (eo,uo)
%                       |--  2a  --|
%                       -----------                      y = 0
%
%
% ------------------------------------------------------ y = -h
% ////////////////////PEC//////////////////////////////
%
% freq = frequency of operation in HERTZ


% h=half seperation of plates
% tol = tolerance of iterative root search
% W = half width of center conductor in METERS (a)
% n = order of Chebyshev polynomial basis functions
% maxIter = max number of Newton-Raphson iterations
%

warning off MATLAB:m_warning_end_without_block

e1=8.8541878176e-12; %F/m ,free space permitivity
u1 = 4*pi*10^-7; %H/m  permiability
eu1=[e1 u1];
k1 = 2*pi*freq*sqrt(e1*u1);
```

```
k = k1;

iter = 2;

del_k=tol*k;
k2=k+del_k;
[A B] = DetImpedMatrix(k, 0, h, W, n, eu1, freq, tol,y_o);
detA = A;
[A B] = DetImpedMatrix(k2, 0, h, W, n, eu1, freq, tol,y_o);
detA2=A;
while iter<maxIter
    p=k2-detA2*(k2-k)/(detA2-detA);
    if abs(p-k)<tol
        prop_const=p;
        impedMat = B;
        break;
    end
    iter=iter+1;
    k=k2;
    detA=detA2;
    k2=p;
    [A B] = DetImpedMatrix(p, 0, h, W, n, eu1, freq, tol,y_o);
    detA2 = A;
end
if iter == maxIter
    disp('Max number of iterations reached');
end
error = abs(detA2*(k2-k)/(detA2-detA));

[Jx, Jz] = PlotCurrents(impedMat, W, n);

end

function [A, B] = DetImpedMatrix(k, del_k, h, W, n, eu1, freq, tol...
    ,y_o)
%
% [A, B] = DetImpedMatrix(k, del_k, l, d, W, n, eu1, eu2, freq, ...
    tol)
%
% DetImpedMatrix returns the determinant of the impedance
% matrix describing the currents on the center conductor of
% the stripline.  It also returns the impedance matrix.
%
% k = propagation constant of stripline
% del_k = propagation constant step for forward difference ...
    calculation
% h= half the distance between parallel plates
% W = length of center conductor in METERS
% n = order of Chebyshev polynomial basis functions
% eu1 = vector containing permittivity and permeability
% freq = frequency of operation in HERTZ
% tol = tolerance of iterative root search
```

```
%
e1 = eu1(1); u1 = eu1(2);

k1 = 2*pi*freq*sqrt(e1*u1);

k = k + del_k;
[A, B, C, D] = EvaluateIntsFormMatrices(k, n, h, W, k1, e1, u1, ...
    tol,y_o);
B = [A B;
     C D];
A = det(B);
end

function [A, B, C, D] = EvaluateIntsFormMatrices(k, n, h, W, k1, ...
    e1, u1,...
     tol,y_o)
%
% [A, B, C, D] = EvaluateIntsFormMatrices(k, n, h, W, k1, e1, u1, ...
    tol,y_o)
%
% EvaluateIntegralsFromMatrices evaluates xi numerical
% integrals and forms the submatrices.
%
% k = propagation constant of stripline
% n = order of Chebyshev polynomial basis functions
% h = half spacing of the groundplanes in METERS
% W = length of center conductor in METERS
% k1 = wavenumber of layer
% e1 = permittivity
% u1 = permeability
% tol = tolerance of iterative root search
% y_o = location of center conductor
%

%%%%% Integration Limits and Tolerance %%%%%
subdiv = 400;     % Number of Subdivisions on Xi Integration ...
    Interval
[limitsXi, tol] = FindIntegrationLimits(k, h, k1, tol, subdiv,y_o)...
    ;
%%%%%%%%%%%%%%%%%%%%%%%%%%%%%%%%%%%%%%%%%%%%%%%%%%%%

for i_test = 0:n - 1
    for i_basis = 0:n - 1
        args = [k W i_test i_basis h k1  e1 u1 y_o ];
        for m = 1:length(limitsXi) - 1
            A1small=(2*1e-4^2-4*1e-4^5)-(2*1e-10^2-4*1e-10^5);
            A1temp(m) = quadl(@EvalIntA1,limitsXi(m),limitsXi(m+1)...
                ,tol,...
                 0,args);

            B1small=(2*1e-4^3)-(2*1e-10^3);
```

```
            B1temp(m) = quadl(@EvalIntB1,limitsXi(m),limitsXi(m+1)...
                ,tol,...
                 0,args);
            D1temp(m) = quadl(@EvalIntD1,limitsXi(m),limitsXi(m+1)...
                ,tol,...
                 0,args);

        end
        A(i_test+1,i_basis+1) = sum(A1temp)+A1small;
        B(i_test+1,i_basis+1) = sum(B1temp)+B1small;
        D(i_test+1,i_basis+1) = sum(D1temp);
    end
end
C=B';
end

function [limitsXi, tol] = FindIntegrationLimits(k, h, k1, tol, ...
    subdiv,y_o)
%
% [limitsXi, tol] = FindIntegrationLimits(k, h, k1, tol, subdiv,...
    y_o)
%
% FindIntegrationLimits finds where the Green's function
% becomes NaN.  It returns the new xi spectral integral
% integration limits and returns an adjusted integration
% tolerance.
%
% k = propagation constant of stripline
% n = order of Chebyshev polynomial basis functions
% h = half spacing of the groundplanes in METERS
% W = length of center conductor in METERS
% k1 = wavenumber of layer
% e1 = permittivity
% u1 = permeability
% tol = tolerance of iterative root search
% y_o = location of center conductor
% subdiv = number of subdivision on xi integration interval
%

tol = tol*1e-6;

xi = 1:1e5;
p1 = sqrt(xi.^2 + k^2 - k1^2);


G1=(cosh(2*p1*h)-cosh(2*p1*y_o))./(p1.*sinh(2*p1*h));


indexNaN1 = find(isnan(G1));
indexZero1 = find(G1==0);
if isempty(indexNaN1) && ~isempty(indexZero1)
    xi_end1 = indexZero1(1) - 1;
```

```
    elseif ~isempty(indexNaN1) && isempty(indexZero1)
        xi_end1 = indexNaN1(1) - 1;
    elseif ~isempty(indexNaN1) && ~isempty(indexZero1)
        if indexNaN1(1) < indexZero1(1)
            xi_end1 = indexNaN1(1) - 1;
        else
            if indexZero1(1) == 1
                xi_end1 = indexNaN1(1) - 1;
            else
                xi_end1 = indexZero1(1) - 1;
            end
        end
    else
        xi_end1 = xi(end);
    end

    limitsXi(:,1) = linspace(1e-4,xi(xi_end1),subdiv);

    end

    function [Jx, Jz] = PlotCurrents(impedMat, W, n)
    %
    % [Jx, Jz] = PlotCurrents(impedMat, W, n)
    %
    % PlotCurrents plots the electric currents on the stripline's ...
       center
    % conductor, Jx and Jz.  It also returns Jx and Jz.
    %
    % impedMat = impedance matrix of stripline environment
    % W = length of center conductor in METERS
    % n = order of Chebyshev polynomial basis functions
    %

    warning off MATLAB:divideByZero

    x = linspace(-W/2,W/2,1000);
    [L,U,P] = lu(impedMat);
    U(end,end) = 0;
    b = inv(P)*L*U;
    as_bs = null(b,'r');
    as = as_bs(1:n);
    bs = as_bs(n+1:end);

    U = ChebyU(n);
    T = ChebyT(n);


    %%%%% Creating Polynomial Representation of Currents %%%%%
    k = 1;
    for i = 1:2:length(T(:,1))
        Jz(k,:) = bs(k)*T(i,:);
        k = k + 1;
```

```
    end
Jz = sum(Jz);
k = 1;
for i = 2:2:length(U(:,1))
    Jx(k,:) = as(k)*U(i,:);
    k = k + 1;
end
Jx = sum(Jx);
Jx = polyval(Jx,2*x/W).*sqrt(1-(2*x/W).^2);
Jz = polyval(Jz,2*x/W)./sqrt(1-(2*x/W).^2);
%%%%%%%%%%%%%%%%%%%%%%%%%%%%%%%%%%%%%%%%%%%%%%%%%%%%%%%%%%%%%%%%%%%%%%%
%%%%% Getting Rid of Inf for Normalization %%%%%
Jztemp = Jz;
Jztemp(1) = '';
Jztemp(end) = '';
%%%%%%%%%%%%%%%%%%%%%%%%%%%%%%%%%%%%%%%%%%%%%%%%%%%%%%%%%%%%%%%%%%%%%%%
JzMag = abs(Jz)/max(abs(Jztemp));
JxMag = abs(Jx)/max(abs(Jztemp));
figure;
plot(2*x/W,JzMag,'-b','Linewidth',2);
hold on;
plot(2*x/W,JxMag,'-.r','Linewidth',2);
xlabel('Location (2x/W)','fontsize',12,'fontweight','bold');
ylabel('Relative Surface Current Magnitude, J_z & J_x','fontsize'...
    ,12,...
    'fontweight','bold');
legend('J_z','J_x');
if mod(n-1,10) == 1
    title_str = [num2str(n-1) '^s^t Order Chebyshev Polynomial ...
       Expansion'];
elseif mod(n,10) == 2
    title_str = [num2str(n-1) '^n^d Order Chebyshev Polynomial ...
       Expansion'];
elseif mod(n,10) == 3
    title_str = [num2str(n-1) '^r^d Order Chebyshev Polynomial ...
       Expansion'];
else
    title_str = [num2str(n-1) '^t^h Order Chebyshev Polynomial ...
       Expansion'];
end
title(title_str,'fontsize',12,'fontweight','bold');
axis tight;
grid on;

end
%%%%%%%%%%%%%%%%%%%%%%%%%%%%%%%%%%%%%%%%%%%%%%%%%%%%%%%%%%%%%%%%%%%%%%%
%%%%%%%%%%%%%%%%%%%%%%%% Integrals %%%%%%%%%%%%%%%%%%%%%%%%%%%%%%%%%%%%
%%%%%%%%%%%%%%%%%%%%%%%%%%%%%%%%%%%%%%%%%%%%%%%%%%%%%%%%%%%%%%%%%%%%%%%
function A = EvalIntA1(xi, args)

k = args(1);
W = args(2); h = args(5);
```

```
    i_test = args(3); i_basis = args(4);
    k1 = args(6);
    y_o=args(9);

291
    p1 = sqrt(xi.^2 + k^2 - k1^2);

    G1=(cosh(2*p1*h)-cosh(2*p1*y_o))./(p1.*sinh(2*p1*h));

296 I1=-j*(-1)^i_basis*(((i_basis+1)*pi)./(W*xi)).*(besselj(2*i_basis...
       +2,xi*W));
    I3=j*(-1)^i_test*(((i_test+1)*pi)./(W*xi)).*(besselj(2*i_test+2,xi...
       *W));


    A = (k1^2 - xi.^2).*G1.*I1.*I3;
301 end

    function A = EvalIntB1(xi, args)
    k = args(1);
    W = args(2); h = args(5);
306 i_test = args(3); i_basis = args(4);
    k1 = args(6);
    y_o=args(9);


311 p1 = sqrt(xi.^2 + k^2 - k1^2);

    G1=(cosh(2*p1*h)-cosh(2*p1*y_o))./(p1.*sinh(2*p1*h));
    I2 = (-1)^i_basis*pi/2*besselj(2*i_basis,xi*W);
    I3 = j*(-1)^i_test*(((i_test+1)*pi)./(W*xi)).*(besselj(2*i_test+2,...
       xi*W));
316
    A = -k*G1.*xi.*I2.*I3;
    end

    function A = EvalIntC1(xi, args)
321 k = args(1);
    W = args(2); h = args(5);
    i_test = args(3); i_basis = args(4);
    k1 = args(6);
    y_o=args(9);
326
    p1 = sqrt(xi.^2 + k^2 - k1^2);
    G1=(cosh(2*p1*h)-cosh(2*p1*y_o))./(p1.*sinh(2*p1*h));
    I1=-j*(-1)^i_basis*(((i_basis+1)*pi)./(W*xi)).*(besselj(2*i_basis...
       +2,xi*W));
    I4=(-1)^i_test*pi/2*besselj(2*i_test,xi*W);
331
    A = -k*G1.*xi.*I1.*I4;
    end
```

```
function A = EvalIntD1(xi, args)
k = args(1);
W = args(2); h = args(5);
i_test = args(3); i_basis = args(4);
k1 = args(6);
y_o=args(9);

p1 = sqrt(xi.^2 + k^2 - k1^2);
G1=(cosh(2*p1*h)-cosh(2*p1*y_o))./(p1.*sinh(2*p1*h));
I2 = (-1)^i_basis*pi/2*besselj(2*i_basis,xi*W);
I4 = (-1)^i_test*pi/2*besselj(2*i_test,xi*W);

A = (k1^2 - k^2)*G1.*I2.*I4;
end

%%%%%%%%%%%%%%%%%%%%%%%%%%%%%%%%%%%%%%%%%%%%%%%%%%%%%%%%%%%%%%%%%%%%%%%
%%%%%%%%%%%%%%%%%%%%%%%%%%%%%%%%%%%%%%%%%%%%%%%%%%%%%%%%%%%%%%%%%%%%%%%
%%%%%%%%%%%%%%%%%%%%%%%%%%%%%%%%%%%%%%%%%%%%%%%%%%%%%%%%%%%%%%%%%%%%%%%
```

Listing B.2: Method of Moment Solution for TEM Specialized Case. (appendix3/TEMChebyCheby12.m)

```
function [impedMat,Jz] = TEMChebyCheby12(freq, h, y_o,tol, W, n)
% based on code developed by Cpt Milo Hyde
%
%
% TEMChebyCheby12 finds the the longitudinal current on the center...
    strip
% of a stripline (Fig-1).  It implements a method of moment ...
    solution that
% expands and tests the currents on the stripline's center ...
    conductor using
% weighted Chebyshev polynomials of the 1st kind.  The algorithm ...
    also
% returns the impedance matrix, the error and the longitudinal ...
    currents
% on the stripline's center conductor, Jz; assuming quasi-TEM, Jx ...
    = 0.
%
% Fig-1
%
% ////////////////////PEC////////////////////////////////
% ------------------------------------------------------  y = h
%  (eo,uo)
%                       |--  2a  --|
%                       -----------                      y = 0
%
%
% ------------------------------------------------------ y = -h
% ////////////////////PEC////////////////////////////////
%
% freq = frequency of operation in HERTZ
% h=half seperation of plates
```

```
% tol = tolerance of iterative root search
% W = length of center conductor in METERS
% n = order of Chebyshev polynomial basis functions
%

warning off MATLAB:m_warning_end_without_block

e1 = 8.8541878176e-12; % F/m (or C2N-1m-2),  free space ...
    permitivity
u1 = 4*pi*10^-7; %H/m (or T m/A) [1] permiability
eu1=[e1 u1];

[A B] = DetImpedMatrix(h, W, n, y_o, eu1, freq, tol);

impedMat = B;
[Jz] = PlotCurrents(impedMat, W, n);

end

function [A, B] = DetImpedMatrix(h, W, n, y_o, eu1, freq, tol)
%
% [A, B] = DetImpedMatrix(k, del_k, l, d, W, n, eu1, eu2, freq, ...
    tol)
%
% DetImpedMatrix returns the determinant of the impedance matrix ...
    describing
% the currents on the center conductor of the stripline.  It also ...
    returns
% the impedance matrix.
%
% freq = frequency of operation in HERTZ
% h=half seperation of plates
% tol = tolerance of iterative root search
% W = length of center conductor in METERS
% n = order of Chebyshev polynomial basis functions
%

e1 = eu1(1); u1 = eu1(2);

k = 2*pi*freq*sqrt(e1*u1);

[B] = EvaluateIntegralsFormMatrices(k, n, h, y_o,W, e1, u1, tol);

A = det(B);
end

function [B] = EvaluateIntegralsFormMatrices(k, n, h, y_o,W, e1, ...
    u1, tol)
%
% [A, B, C, D] = EvaluateIntegralsFormMatrices(k, n, h, y_o,W, e1,...
    u1, tol)
%
```

```
% EvaluateIntegralsFromMatrices evaluates xi numerical integrals ...
    and forms
% the submatrices.
%
% freq = frequency of operation in HERTZ
% h=half seperation of plates
% tol = tolerance of iterative root search
% W = length of center conductor in METERS
% n = order of Chebyshev polynomial basis functions
%

%%%%% Integration Limits and Tolerance %%%%%
subdiv = 400;     % Number of Subdivisions on Xi Integration ...
    Interval
k1=k;
[limitsXi, tol] = FindIntegrationLimits(k, h, k1, tol, subdiv);
%%%%%%%%%%%%%%%%%%%%%%%%%%%%%%%%%%%%%%%%%%%%%%%%%%%%%%%%%%%%
%limitsXilarge=linspace(limitsXi(end),100000,subdiv);
%limitsXi=linspace(1e-4,150000,subdiv);
for i_test = 0:n - 1
    for i_basis = 0:n - 1
        args = [k W i_test i_basis h e1 u1 y_o ];
        for m = 1:length(limitsXi) - 1
            B1small=(2*1e-4^3)-(2*1e-10^3);
            B1temp(m) = quadl(@EvalIntB1,limitsXi(m),limitsXi(m+1)...
                ,...
                 tol,0,args);
        end

        B(i_test+1,i_basis+1) = sum(B1temp)+B1small;

    end
end

end

function [limitsXi, tol] = FindIntegrationLimits(k, h, k1, tol, ...
    subdiv)
%
% [limitsXi, tol] = FindIntegrationLimits(k, l, d, k1, k2, e1, u1,...
    e2, u2, tol, subdiv)
%
% FindIntegrationLimits finds where the Green's function becomes ...
    NaN.  It
% returns the new xi spectral integral integration limits and ...
    returns an
% adjusted integration tolerance.
%
% freq = frequency of operation in HERTZ
% h=half seperation of plates
% tol = tolerance of iterative root search
% W = length of center conductor in METERS
```

```
% n = order of Chebyshev polynomial basis functions
%
%

tol = tol*1e-6;

xi = 1:1e5;
p1 = sqrt(xi.^2 + k^2 - k1^2);


G1=(cosh(2*p1*h)-cosh(2*p1*0))./(p1.*sinh(2*p1*h));


indexNaN1 = find(isnan(G1));
indexZero1 = find(G1==0);
if isempty(indexNaN1) && ~isempty(indexZero1)
    xi_end1 = indexZero1(1) - 1;
elseif ~isempty(indexNaN1) && isempty(indexZero1)
    xi_end1 = indexNaN1(1) - 1;
elseif ~isempty(indexNaN1) && ~isempty(indexZero1)
    if indexNaN1(1) < indexZero1(1)
        xi_end1 = indexNaN1(1) - 1;
    else
        if indexZero1(1) == 1
            xi_end1 = indexNaN1(1) - 1;
        else
            xi_end1 = indexZero1(1) - 1;
        end
    end
else
    xi_end1 = xi(end);
end

limitsXi(:,1) = linspace(1e-4,xi(xi_end1),subdiv);

end


function [Jz] = PlotCurrents(impedMat, W, n)
%
% [Jz] = PlotCurrents(impedMat, W, n)
%
% PlotCurrents plots the electric currents on the stripline's ...
   center
% conductor, Jz.  It also returns Jx and Jz.
%
% impedMat = impedance matrix of stripline environment
% W = length of center conductor in METERS
% n = order of Chebyshev polynomial basis functions
%

warning off MATLAB:divideByZero
```

```
168
    x = linspace(-W/2,W/2,1000);
    [L,U,P] = lu(impedMat);
    U(end,end) = 0;
    b = inv(P)*L*U;
173 as = null(b,'r');



    U = ChebyU(n);
178 T = ChebyT(n);


    %%%%% Creating Polynomial Representation of Currents %%%%%
    k = 1;
183 for i = 1:2:length(T(:,1))
        Jz(k,:) = as(k)*T(i,:);
        k = k + 1;
    end
    Jz = sum(Jz);
188
    Jz = polyval(Jz,2*x/W)./sqrt(1-(2*x/W).^2);
    %%%%%%%%%%%%%%%%%%%%%%%%%%%%%%%%%%%%%%%%%%%%%%%%%%%%%%%%%%%%%%%%
    %%%%% Getting Rid of Inf for Normalization %%%%%
    Jztemp = Jz;
193 Jztemp(1) = '';
    Jztemp(end) = '';
    %%%%%%%%%%%%%%%%%%%%%%%%%%%%%%%%%%%%%%%%%%%%%%%%%%%%%%%%%%%%%%%%
    JzMag = abs(Jz)/max(abs(Jztemp));

198 set(0, 'defaulttextinterpreter', 'latex');
    f = figure(2); plot(2*x/W, JzMag, 'LineWidth', 2);
    set(gca, 'Units', 'Inches', 'OuterPosition', [0 0.5 5 0.5+2]);
    set(f, 'Units', 'Inches', 'PaperPosition', [1 1 5 4]);
    grid('on');
203 xlabel('\centerline{Location (2x/W)}', 'FontSize', 12);
    ylabel('Relative Surface Current Magnitude, J_z ', 'FontSize', 12)...
        ;
    title({'\centerline{Current through }'; '\centerline{TEM ...
        Specialization}'}, 'FontSize', 12);
    set(gca, 'fontname', 'times');
    print('-depsc', 'TEMcurrent');
208
    end

    %...
        %%%%%%%%%%%%%%%%%%%%%%%%%%%%%%%%%%%%%%%%%%%%%%%%%%%%%%%%%%%%%%%%...

    %%%%%%%%%%%%%%%%%%%%%%%% Integrals ...
        %%%%%%%%%%%%%%%%%%%%%%%%%%%%%%%%
```

```
213 %...
    %%%%%%%%%%%%%%%%%%%%%%%%%%%%%%%%%%%%%%%%%%%%%%%%%%%%%%%%%%%%%%%%%%%%...


    function A = EvalIntB1(xi, args)

    k = args(1);
218 W = args(2); h = args(5);
    i_test = args(3); i_basis = args(4);
    k1 = args(1);
    y_o=args(8);

223
    p1 = sqrt(xi.^2 + k^2 - k1^2);
    G1=(cosh(2*p1*h)-cosh(2*p1*y_o))./(p1.*sinh(2*p1*h));
    I2=(-1)^i_basis*pi/2*besselj(2*i_basis,xi*W);%gz
    I3=j*(-1)^i_test*(((i_test+1)*pi)./(W*xi)).*(besselj(2*i_test+2,xi...
       *W));%fx
228
    A = -k*G1.*xi.*I2.*I3;
    end


233 %...
    %%%%%%%%%%%%%%%%%%%%%%%%%%%%%%%%%%%%%%%%%%%%%%%%%%%%%%%%%%%%%%%%%%%%...

    %...
    %%%%%%%%%%%%%%%%%%%%%%%%%%%%%%%%%%%%%%%%%%%%%%%%%%%%%%%%%%%%%%%%%%%%...

    %...
    %%%%%%%%%%%%%%%%%%%%%%%%%%%%%%%%%%%%%%%%%%%%%%%%%%%%%%%%%%%%%%%%%%%%...
```

Listing B.3: Algorithm for computing Chebsyshev Polynomials of the First Kind (appendix3/ChebyT.m)

```
function [T] = ChebyT(n)
%%%%% Generates Chebyshev Polynomials of the 1st Kind %%%%%
T = zeros(2*n,2*n);
for i = 0:2*n - 1
 5     if i == 0
           T(1,2*n) = 1;
       elseif i == 1
           T(2,2*n-1) = 1;
       else
10         T(i+1,:) = 2*circshift(T(i,:),[0 -1]) - T(i-1,:);
       end
end
%%%%%%%%%%%%%%%%%%%%%%%%%%%%%%%%%%%%%%%%%%%%%%%%%%%%%%%%%%%%%%%%%%%%%%%
```

Listing B.4: Algorithm for computing Chebsyshev Polynomials of the Second Kind (appendix3/ChebyU.m)

```
function [T] = ChebyU(n)
%%%%% Generates Chebyshev Polynomials of the 1st Kind %%%%%
T = zeros(2*n,2*n);
for i = 0:2*n - 1
    if i == 0
        T(1,2*n) = 1;
    elseif i == 1
        T(2,2*n-1) = 2;
    else
        T(i+1,:) = 2*circshift(T(i,:),[0 -1]) - T(i-1,:);
    end
end
%%%%%%%%%%%%%%%%%%%%%%%%%%%%%%%%%%%%%%%%%%%%%%%%%%%%%%%%%%%%%%%%%%%%%%%
```

# *Bibliography*


1. Akan, Volkan. "Quasistatic TEM analyses of elliptical, cylindrical, and asymmetric shielded striplines: Multilayered case". *International Journal of RF and Microwave Computer-Aided Engineering*, 16(2):181, 2008.

2. Amano, Y.; Minaguchi Y.; Tsujimoto H., M.; Tamigawa and K. Shirae. "A method permeability measurement of magnetic thin film in the GHz region". *Magnetics Conference, 1992. Digests of Intermag '92., International*, 150–150, Apr 1992.

3. Arfken, George B. *Mathematical methods for physicists*. Academic Press, New York, third edition, 1985.

4. Bagby, Lee C.-H. Yuan Y., J.S. and D.P. Nyquist. "Entire-domain basis MOM analysis of coupled microstrip transmission lines". *Microwave Theory and Techniques, IEEE Transactions on*, 40(1):49–57, Jan 1992. ISSN 0018-9480.

5. Balanis, Constantine A. *Advanced Engineering Electromagnetics*. John Wiley & Sons, Inc., New York, NY, second edition, 1989.

6. Barry, Walter. "A Broad-Band, Automated, Stripline Technique for the Simultaneous Measurement of Complex Permittivity and Permeability". *IEEE Transactions on Microwave Theory and Techniques*, 34(1):80–84, January 1986.

7. Beyer, W.H. *CRC Standard Mathematical Tables*. CRC Press, 27th edition, 1984.

8. Boas, Mary L. *Mathematical Methods in the Physical Sciences*. John Wiley & Sons, Inc., third edition, 2006.

9. Chen, C. K. Ong C. P. Neo V. V. Varadan, L. F. and Vijay K. Varadan. *Microwave electronics : measurement and materials characterisation*. Imprint Chichester : John Wiley, Mass., 2004.

10. Cohn, Seymour B. "Charcteristic Impedance of the Shielded-Strip Transmission Line". *IEEE Transactions on Microwave Theory and Techniques*, 2:52–57, July 1954.

11. Collin, Robert E. *Field theory of guided waves*. Artech House, New York, 1991.

12. Dvorak, Steven L. "Applications for Incomplete Lipschitz-Hankel Integrals in Electromagnetics". *IEEE Transactions on Antennas and Propagation*, 36(6):26–32, Dec 1994.

13. Dvorak, Steven L. and Edward F. Kuester. "Numerical Computation of the Incomplete Lipschitz-Hankel Integrals Jeo(a,z)". *Journal of Computational Physics*, 87:301–327, Dec 1990.

14. Frenkel, A. "On entire-domain basis functions with square-root edge singularity [EM scattering]". *Antennas and Propagation, IEEE Transactions on*, 37(9):1211–1214, Sep 1989. ISSN 0018-926X.

15. Gunsaya, Terry Golds Philip J. Page Michael J. Bosley, Ayhan and John F. Dawson. "Analysis of Tri-plate Line, SAE J1113-25, using CAE tools". *Institute of Electrical and Electronics Engineers (IEEE)*, (3):626–631, June.

16. Hanson, Jerry M. Grimm, George W. and Dennis P. Nyquist. "An Improved De-embedding Technique for the Measurement of the Complex Constitutive Parameters of Materials Using Stripline Field Applicator". 42(3):740–745, June 1993.

17. Havrilla, M. J. *Analytical and Experimental Techniques for the Electromagnetic Characterization of Materials*. Ph.D. thesis, Michigan State University, 2001.

18. Havrilla, M. J. and D. P Nyquist. "Electromagnetic Characterization of Layered Materials via Direct and De-embed Methods". *IEEE Trans. on Instramentation and Measurement*, 55(1):158–163, Feb 2006.

19. Havrilla, Micheal. "EENG622 Electromagnetics Class Notes", Oct 2007. EENG622 Electromagnetics.

20. Howe, Harlan. *Stripline circuit design*. Artech House, Mass., 1974.

21. Hwang, Ruey Bing. *Institute of Electrical and Electronics Engineers (IEEE)*.

22. Infante, D. J. *Full-wave integral-operator description of propagation modes excited on stripline structures*. Ph.D. thesis, MICHIGAN STATE UNIVERSITY, 1999.

23. Iskander, Madgy F. *Electric Fields and Waves*. Waveland Press, Inc., Prospect Heights, Illinois, 1992.

24. Johansson, Joachim and Urban Lundgren. *EMC of Telecommunication Lines*. Master's thesis, LuLea University of Technology, 1997.

25. Kammler, D.W. "Calculation of Characteristic Admittances and Coupling Coefficients for Strip Transmission Lines". *IEEE Transactions on Microwave Theory and Techniques*, 16(11):925–937, Dec 1968.

26. Levy, R. "New Coaxial-to-Stripline Transformers Using Rectangular Lines". *IEEE Transactions on Microwave Theory and Techniques*, 273–274, May 1961.

27. Li, Huadong. "The Field Distribution of a tri-plate and its Influence on the Immunity Test". *Institute of Electrical and Electronics Engineers (IEEE)*, (3):85–88, June.

28. Nyquist, J. M. Grimm D. J. Infante, D. P. and H. Braunisch. "Classification of the Proper Propagation-Mode Spectrum and Leaky-Wave Modes on Open Planar Waveguides". *Electromagnetics*, 17:105–130, September 1997.

29. Peterson, Scott L. Ray, Andrew F. and Raj Mittra. *Computational methods for electromagnetics*. IEEE Press ; Oxford : Oxford University Press, New York, NY, 1998.

30. Polonis, William E. Cory Ismeal Martinez Jr. David A. Smith, James J. and Herbert H. Walker. "Tri-Plate Test Fixture". *Institute of Electrical and Electronics Engineers (IEEE)*, 153–158, May 1998.

31. Pozar, David M. *Microwave engineering*. Addison-Wesley, New York, NY, second edition, 1990.

32. Pyle, J. R. "Broad-band Coaxial-to-Stripline Transitions". *IEEE Transactions on Microwave Theory and Techniques*, 364–365, Febuary 1964.

33. Rivlin, T.J. *The Chebyshev Polynomials*. John Wiley & Sons, New York, 1974.

34. Salahun, Patric Queffelec Marcel Le Floc'h, Erwin and Philippe Gelin. "A Broadband Permeameter for the "in situ" Measurements of Rectangular Samples". *IEEE Transactions on Magnetics*, 37(4):2743–2745, July 2001.

35. Scogna, A.C. and M. Schauer. "Stripline Simulation Model with Tapered Cross Section and Conductor Surface Profile". *Electromagnetic Compatibility, 2007. EMC 2007. IEEE International Symposium on*, 1–5, July 2007.

36. Strange, Gilbert. *Introduction to Linear Algrebra*. Wellesley-Cambridge Press, New York, NY, second edition, 1998.

37. Vegni, Alessandro Toscano, Lucio and Filiberto Bilotti. "Tapered Stripline Embedded in Inhomogeneous Media as Microwave Matching Line". *IEEE Transactions on Microwave Theory and Techniques*, 49(5):970–978, May 2001.

38. Wang, Sutirtha Kabir John Weber, Xing and Steven L. Dvorak. "A Study of the Fields Associated With Horizontal Dipole Sources in Stripline Circuits". 25(2):280–287, May 2002.

39. Zelinski, Gregory M. and Derek Dwyer. "Summary of EENG624 Labs 2 and 3: Determining a Maretial's Constitutive Parameters with Stripline Measurements", June 2008. EENG624 Material Measurements.

# *Index*

The index is conceptual and does not designate every occurrence of a keyword. Page numbers in bold represent concept definition or introduction.

# REPORT DOCUMENTATION PAGE

*Form Approved*
*OMB No. 0704–0188*



| 1. REPORT DATE *(DD–MM–YYYY)* | 2. REPORT TYPE | 3. DATES COVERED *(From — To)* |
|---|---|---|
| 19–03–2009 | Master's Thesis | Sept 2007 — Mar 2009 |

**4. TITLE AND SUBTITLE**

Full-Wave Based Validation
of Stripline Field Applicator
For Low Frequency
Material Measurements

**5a. CONTRACT NUMBER**

DACA99–99–C–9999

**5b. GRANT NUMBER**

**5c. PROGRAM ELEMENT NUMBER**

**6. AUTHOR(S)**

James H. Crane, II, Capt, USAF

**5d. PROJECT NUMBER**

09164

**5e. TASK NUMBER**

**5f. WORK UNIT NUMBER**

**7. PERFORMING ORGANIZATION NAME(S) AND ADDRESS(ES)**

Air Force Institute of Technology
Graduate School of Engineering and Management (AFIT/EN)
2950 Hobson Way
WPAFB OH 45433-7765

**8. PERFORMING ORGANIZATION REPORT NUMBER**

AFIT/GE/ENG/09-10

**9. SPONSORING / MONITORING AGENCY NAME(S) AND ADDRESS(ES)**

Air Force Research Laboratory
ATTN: Garrett Stenholm
2591 K Street
Area B, Bldg 254
Wright Patterson AFB, OH 45303
((937)255–9179 Garrett.Stenholmwpafb.af.mil)

**10. SPONSOR/MONITOR'S ACRONYM(S)**

AFRL/RYS (AFMC)

**11. SPONSOR/MONITOR'S REPORT NUMBER(S)**

**12. DISTRIBUTION / AVAILABILITY STATEMENT**

Approval for public release; distribution is unlimited.

**13. SUPPLEMENTARY NOTES**

**14. ABSTRACT**

This research presents the analysis and verification of a stripline designed by Air Force Research Laboratory for use in measuring the electrical properties of materials at low frequencies and high temperature. It is designed to operate in the TEM mode up to 4 Ghz and have a characteristic impedance of 50 ohms. A full wave base method is used to analyze the structure. A pair of coupled electric field integral equations (CIE) are formulated using The parallel plate waveguide dyadic Green's function. These CIEs are solved through a computationally efficient entire-domain method of moments (MoM) technique. Numerical efficiency are gained through employing Chebsyshev polynomials of the first and second kind as testing and expansion functions. Further numerical efficiencies are gained by taking advantage of transverse electromagnetic propagation properties to develop a specialized TEM integral equation. An expression for the characteristic impedance is developed using the MoM results. The characteristic impedance is calculated for various degrees of center conductor miss alignment.

**15. SUBJECT TERMS**

Green's function, integral equation, Method of Moments, Chebsyshev polynomial, Characteristic impedance, misaligned stripline

| 16. SECURITY CLASSIFICATION OF: | | | 17. LIMITATION OF ABSTRACT | 18. NUMBER OF PAGES | 19a. NAME OF RESPONSIBLE PERSON |
|---|---|---|---|---|---|
| a. REPORT | b. ABSTRACT | c. THIS PAGE | | | Dr. Michael J. Havrilla, PHD |
| U | U | U | UU | 99 | 19b. TELEPHONE NUMBER *(include area code)* (937)255–3636, x 4582; micharl.havrilla@afit.edu |